nature communications

Article

https://doi.org/10.1038/s41467-025-61094-5

# Scalable modulation of CRISPR–Cas enzyme activity using photocleavable phosphorothioate DNA

Received: 21 November 2024

Accepted: 12 June 2025

Published online: 01 July 2025

Check for updates

Menglu Hu[1,8], Bingni Zhang[1,8], Yuanyue Shan[2,8], Feng Cao[1], Yihui Wang[1], Weiwei Qi[1], Xue Wang[1], Yuting Shen[1], Xinyi Guo[1], Mengmeng Zhang[3], Tian Tian[1], Wei Xie[4], Mingfeng Zhang[3,5] ✉, Fang Liang[1,6] ✉, Duanqing Pei[3,5] ✉ & Xiaoming Zhou[1,7] ✉

The regulation of CRISPR–Cas activity is critical for developing advanced biotechnologies. Optical control of CRISPR–Cas system activity can be achieved by modulation of Cas proteins or guide RNA (gRNA), but these approaches either require complex protein engineering modifications or customization of the optically modulated gRNAs according to the target. Here, we present a method, termed photocleavable phosphorothioate DNA (PC&PS DNA)-mediated regulation of CRISPR–Cas activity (DNACas), that is versatile and overcomes the limitations of conventional methods. In DNACas, CRISPR–Cas activity is silenced by the affinity binding of PC&PS DNA and restored through light-triggered chemical bond breakage of PC&PS DNA. The universality of DNACas is demonstrated by adopting the PC&PS DNA to regulate various CRISPR–Cas enzymes, achieving robust light-switching performance. DNACas is further adopted to develop a light-controlled one-pot LAMP-BrCas12b detection method and a spatiotemporal gene editing strategy. We anticipate that DNACas could be employed to drive various biotechnological advances.

The advent of clustered regularly interspaced short palindromic repeat (CRISPR)-associated protein (Cas) systems and the development of their applications in gene editing, regulation, and diagnostics are among the most exciting innovations in the biotechnology field in recent years[1–6]. The regulation of CRISPR–Cas activity is highly beneficial because certain nonspecific enzymatic reactions can be detrimental to many biological applications. For example, controlling enzyme activity in CRISPR diagnostics is an excellent solution to address the incompatibility problem between CRISPR cleavage and nucleic acid amplification[7–9]. For gene-editing development, controlling CRISPR–Cas9 activity is crucial for developing site-specific gene editing or minimizing off-target effects[10–12]. Overall, precise regulation of CRISPR–Cas system activity broadens its application in scientific research and accelerates its practical use in clinical and industrial fields.

Light is ideal for providing high spatial and temporal resolution in regulating CRISPR–Cas activity. Several methods are available for

[1]School of Life sciences, South China Normal University, Guangzhou, China. [2]Centre for Regenerative Medicine and Health, Hong Kong Institute of Science & Innovation, Chinese Academy of Sciences, Hong Kong SAR, China. [3]Laboratory of Cell Fate Control, School of Life Sciences, Westlake University, Hangzhou, China. [4]MOE Key Laboratory of Gene Function and Regulation, State Key Laboratory for Biocontrol, School of Life Sciences, Sun Yat-Sen University, Guangzhou, Guangdong, People's Republic of China. [5]Westlake Laboratory of Life Sciences and Biomedicine, Hangzhou, Zhejiang, China. [6]Institute of Modern Aquaculture Science and Engineering, School of Life Sciences, South China Normal University, Guangzhou, China. [7]MOE Key laboratory of Laser Life Science & Guangdong Provincial Key Laboratory of Laser Life Science, School of Optoelectronic Science and Engineering, South China Normal University, Guangzhou, China. [8]These authors contributed equally: Menglu Hu, Bingni Zhang, Yuanyue Shan. ✉e-mail: zhangmingfeng@westlake.edu.cn; rachel8l@m.scnu.edu.cn; peiduanqing@westlake.edu.cn; zhouxm@scnu.edu.cn

optical control of CRISPR–Cas activity[11,13–16]. Typically, the CRISPR–Cas system is silenced by the site-specific installation of a photocaged amino acid, and the activity can be restored when the photocaged group is removed by light[17]. In other cases, light control of CRISPR–Cas system activity is achieved by photoinducible dimerization or isomerization[16,18,19]. While these methods work effectively, the following issues need to be addressed. i. Understanding the structural details in advance and executing time-consuming trial-and-error protein engineering and screening is necessary. ii. There is a lack of general guidelines for developing new light-controlled enzymes. iii. Enzyme activity recovery is usually inefficient due to structural disturbance caused by protein engineering. Some light-controlled CRISPR–Cas enzymes are also developed by optically regulating guide RNA (gRNA) activity[20–25], circumventing the need for protein engineering procedures and trial-and-error screening processes. However, the light-regulated gRNA used in this approach is highly dependent on chemical synthesis, making it unsuitable for other long-stranded gRNAs that are difficult to synthesize chemically, such as the gRNA of the Cas12b and Cas12f system. Furthermore, the need for customized synthesis of light-regulated gRNA based on specific targets poses a generalizability issue. Consequently, developing simpler photoregulation methods that are universal to other CRISPR–Cas systems remains a challenge.

Phosphorothioate (PS) containing DNA (PS DNA) is a chemically modified nucleic acid in which a non-bridging oxygen atom in the nucleotide backbone is replaced by a sulfur atom. This modification enhances DNA stability and preserves its biological activity. PS DNA demonstrates high-affinity and broad protein-binding capability, including interactions with plasma proteins, cell-surface proteins, and intracellular proteins[26]. Mechanistic studies using human positive cofactor 4 (PC4) as a model reveal PS DNA binding to the protein through electrostatic and hydrophobic interactions[27]. Specifically, studies on the Ff gene 5 protein show that PS DNA binds to the protein with approximately 300-fold higher affinity than natural phosphodiester DNA (PO DNA)[28]. Additionally, experiments demonstrate that PS DNA binding to LbCas12a significantly inhibits its activity[29,30]. This broad protein affinity, robust binding stability, and inhibitory effect on protein activity position PS DNA as a potential tool for regulating CRISPR–Cas protein activity.

In parallel, photocleavable linkers (PC-linkers) are widely employed for light-mediated control of nucleic acid function due to their efficient and predictable bond cleavage under specific wavelengths of light[31]. Among them, ortho-nitrobenzyl (ONB) derivatives represent one of the most extensively used and commercially available PC-linkers[32,33]. Upon exposure to near-ultraviolet (UV) light (365 nm), ONB groups undergo rapid photolysis, typically completing cleavage within seconds to minutes. Moreover, PC-linkers offer several advantages, including synthetic accessibility, biological compatibility, and ease of integration into oligonucleotides. These features make PC-linkers an effective candidate for constructing light-responsive CRISPR–Cas tools[7,21,34].

In this study, we develop a more convenient way to achieve optical control of the CRISPR–Cas system. In the method development process, we verify a key mechanism whereby DNA sequences with varied PS modifications significantly correlate with their inhibiting effect on CRISPR–Cas activity. Building upon this discovery, we embed ONB derivatives-based PC-linkers into PS DNA to obtain photocleavable phosphorothioate DNA (PC&PS DNA), whose chemical bonds can be broken by light irradiation. Interestingly, among the tested CRISPR–Cas enzymes, PC&PS DNA almost completely inhibits enzyme activity (~100%), and flexible regulation of enzymatic activity can be achieved with a short photoirradiation step (1 min). This mechanism allows us to develop a light-controlled tool, termed PC&PS DNA-mediated regulation of CRISPR–Cas activity (DNACas). Compared with conventional methods, DNACas is simple and versatile, eliminating the need for protein engineering and trial-and-error screening. Additionally, its versatility and effectiveness are maintained even with diverse gRNA transformations. We employ DNACas to build a light-controlled one-pot loop-mediated isothermal amplification (LAMP)-BrCas12b assay (light-controlled one-pot assay) and a spatiotemporal gene editing strategy. We anticipate that DNACas could lead to advancements in various biotechnologies.

## Results

### PS DNA-mediated LbCas12a activity inhibition

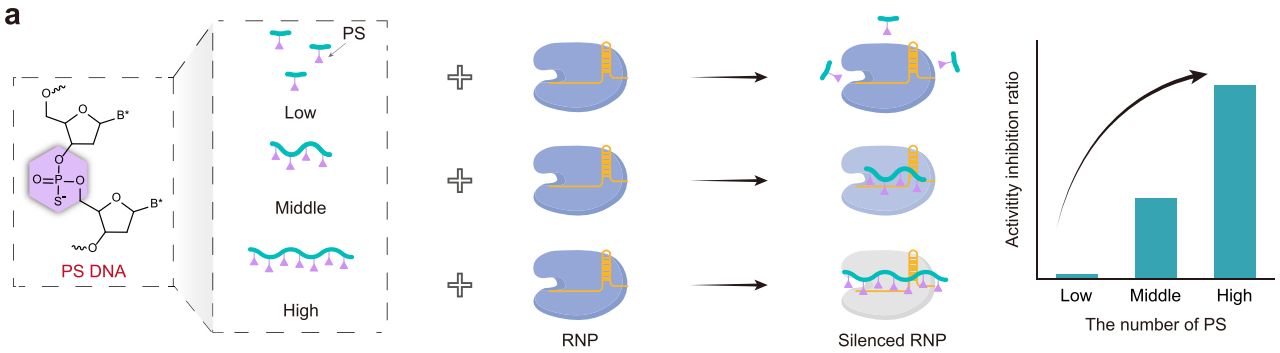
PS DNA has been found to exist in a natural form in bacteria[35]. Chemically synthesized PS DNA is also widely used in nucleic acid therapeutics for improving pharmacological properties[26,36,37]. Compared to PO DNA, PS DNA is more resistant to nuclease degradation and more easily taken up by cells[36,38–40]. In addition, studies have shown that PS DNA exhibits broad protein-binding affinity and inhibitory effects[26,27,41–43], including its inhibitory and binding effects on the *cis*-cleavage activity of LbCas12a[29,30], which is responsible for the specific recognition and cleavage of the target[44].

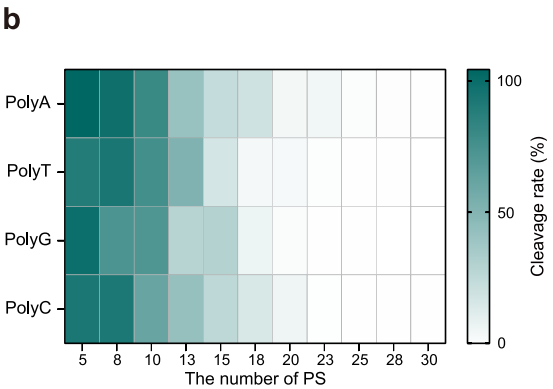
Here, we evaluated the impact of varying levels of PS modifications in DNA sequences on the activity of the CRISPR–Cas system (Fig. 1a). A group of PS DNA sequences with different amounts of PS modification were employed to evaluate their inhibitory effect on LbCas12a *trans*-cleavage activity in vitro (Fig. 1b). These PS DNAs consisted of poly A, poly T, poly G, and poly C bases, respectively, with varied lengths (Supplementary Data 1). We incubated these sequences with ribonucleoprotein (RNP) complexes formed by LbCas12a and crRNA for 5 min and subsequently measured the LbCas12a *trans*-cleavage activity by a fluorescence-based assay. Upon activation, the *trans*-cleavage activity of LbCas12a nonspecifically cleaves the fluorescent quencher (FQ) C6 probe, generating fluorescence as an indicator of enzymatic activity[44]. It was found that the inhibitory efficiency of PS DNA on LbCas12a was positively correlated with the number of PS modifications in DNA sequences, and it exhibited no base dependence. To further investigate the underlying mechanism, we employed biolayer interferometry (BLI) to accurately determine the binding affinity between PS DNA, PO DNA, and LbCas12a (Fig. 1c). The experimental results showed that the presence of PS modifications in nucleic acid sequences enhanced their binding affinity with LbCas12a, showing a trend corresponding to the number of PS modifications in DNA sequences. Further tests using a set of DNAs with random base composition and varying numbers and positions of PS modification showed that the inhibitory effect depends on the total number of PS modifications rather than base composition or modification position (Fig. 1d).

### In vitro development of the DNACas assay

This PS modification number-dependent inhibition mechanism motivated us to develop a light-controlled method for regulating enzyme activity, termed DNACas. The ONB type PC-linker was embedded into the PS DNA to create PC&PS DNA, whose length could be controlled by light-triggered DNA breakage. The binding of PC&PS DNA to the RNP can effectively inhibit its activity until exposure to UV light, which induces a breakage in chemical bond of PC&PS DNA (Fig. 2a). Subsequently, we evaluated the impact of the number of PC-linkers in PC&PS DNA on their light-switching efficiency with LbCas12a enzyme (Fig. 2b). A series of PC&PS DNAs were designed with 25 PS modifications, random base composition, and varied PC-linker numbers. The results showed that all sequences effectively inhibited LbCas12a activity, irrespective of the number of PC-linker modifications. Notably, light-mediated recovery of enzyme activity increased proportionally with the number of PC-linkers. When 12 PC-linkers were incorporated, over 80% of enzyme activity was restored. Similar patterns were observed when these sequences were used to regulate the *trans*-cleavage of LbuCas13a[45], as well as the *cis*-cleavage activities of LbCas12a (Fig. 2c, d). These findings

https://doi.org/10.1038/s41467-025-61094-5




c

| Name | Sequences | $K_D$ (M) |
|---|---|---|
| 20PS 21nt | 5′ Biotin- G C G A C T C G G T T C T T G C C T A A G 3′ | $6.95 \times 10^{-9}$ |
| 15PS 21nt | 5′ Biotin- G C G A C T C G G T T C T T G C C T A A G 3′ | $9.26 \times 10^{-9}$ |
| 10PS 21nt | 5′ Biotin- G C G A C T C G G T T C T T G C C T A A G 3′ | $1.15 \times 10^{-8}$ |
| 5PS 21nt | 5′ Biotin- G C G A C T C G G T T C T T G C C T A A G 3′ | $1.62 \times 10^{-8}$ |
| 15PS 16nt | 5′ Biotin- T C G G T T C T T G C C T A A G 3′ | $7.39 \times 10^{-9}$ |
| 10PS 11nt | 5′ Biotin- T C T T G C C T A A G 3′ | $1.48 \times 10^{-8}$ |
| 5PS 6nt | 5′ Biotin- C C T A A G 3′ | $2.92 \times 10^{-8}$ |
| PO 21nt | 5′ Biotin- G C G A C T C G G T T C T T G C C T A A G 3′ | $1.36 \times 10^{-8}$ |
| PO 16nt | 5′ Biotin- T C G G T T C T T G C C T A A G 3′ | $1.57 \times 10^{-8}$ |
| PO 11nt | 5′ Biotin- T C T T G C C T A A G 3′ | $4.06 \times 10^{-8}$ |
| PO 6nt | 5′ Biotin- C C T A A G 3′ | $7.67 \times 10^{-8}$ |

PS modification

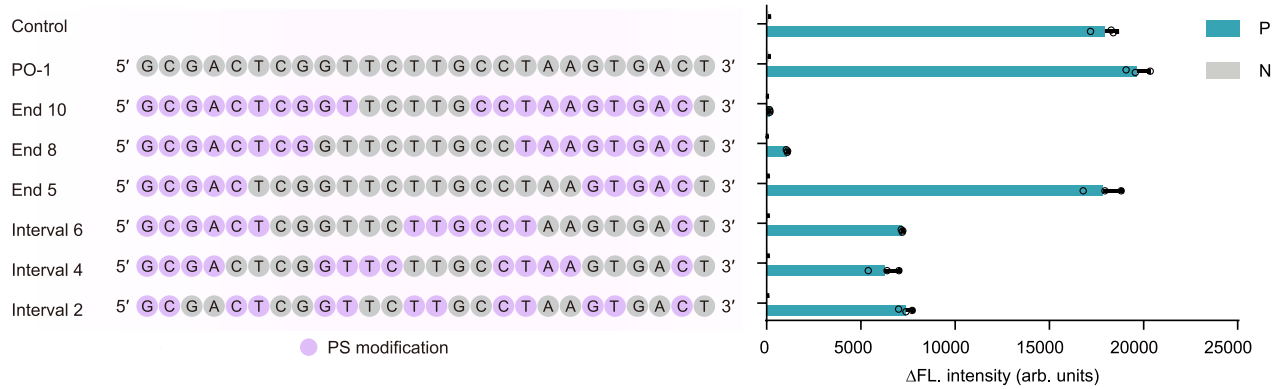



**Fig. 1 | In vitro analysis of CRISPR–Cas12a activity inhibition mediated by different PS DNAs. a** Schematic diagram of CRISPR–Cas12a activity inhibition mediated by PS DNA with different numbers of PS modifications. **b** Effects of different PS modification numbers of poly(A), poly(T), poly(G), and poly(C) DNA on LbCas12a activity were measured. The cleavage rate was calculated by comparison to the native LbCas12a for detecting the same target DNA. LbCas12a activity was measured based on the *trans*-cleavage of an FQ probe. The final concentration of PS DNA in the reaction system is 100 nM. The final concentration of the LbCas12a is 15 nM. The total length of the DNA sequences corresponds to the number of PS modifications plus one. **c** The dissociation constants of LbCas12a with PS DNA and PO DNA determined by BLI. The bases modified with PS are highlighted in purple. **d** Evaluating the inhibitory ability of PS DNA with varied PS modification content and position on the LbCas12a activity. All DNA sequences have the same base composition. The PO-1 sequence contains no PS modifications. The PS modification content and position are highlighted in purple in the other six sequences. Control represents the LbCas12a assay without adding PS or PO DNA to the reaction system. The final concentration of these DNA sequences in the reaction system is 60 nM. *P* represents the positive group using double-stranded DNA (dsDNA) as the target, while *N* represents the blank control with RNase-free water as the target. ΔFL. Intensity represents the difference between the 60 min and initial fluorescence values. Data are represented as mean ± standard error ($n = 3$ technical replicates). Source data are provided as a Source Data file.

suggest that Cas protein activity can be flexibly modulated by introducing PS DNA containing varying amounts of PC-linkers. The concentration-dependent experiments using four PC&PS DNAs with poly A, poly T, poly G, and poly C bases, along with one 25PS12PC DNA with random sequence, demonstrated that effective photoswitchable LbCas12a activity required a higher concentration of PC&PS DNAs than that of the LbCas12a protein (Supplementary Fig. 1). We further tested the detailed impact of the base composition and length of PC&PS DNA on the LbCas12a activity inhibition performance, demonstrating that the concentration of PC&PS DNA required to completely inhibit LbCas12a activity decreased as the length of the PC&PS DNA increased and has no base dependence (Fig. 2e, f,). Furthermore, we evaluated the stability of PC&PS DNA under ambient light and observed no significant activation after 8 h of exposure, confirming that the photochemical activation process was wavelength-selective (Supplementary Fig. 2).

https://doi.org/10.1038/s41467-025-61094-5

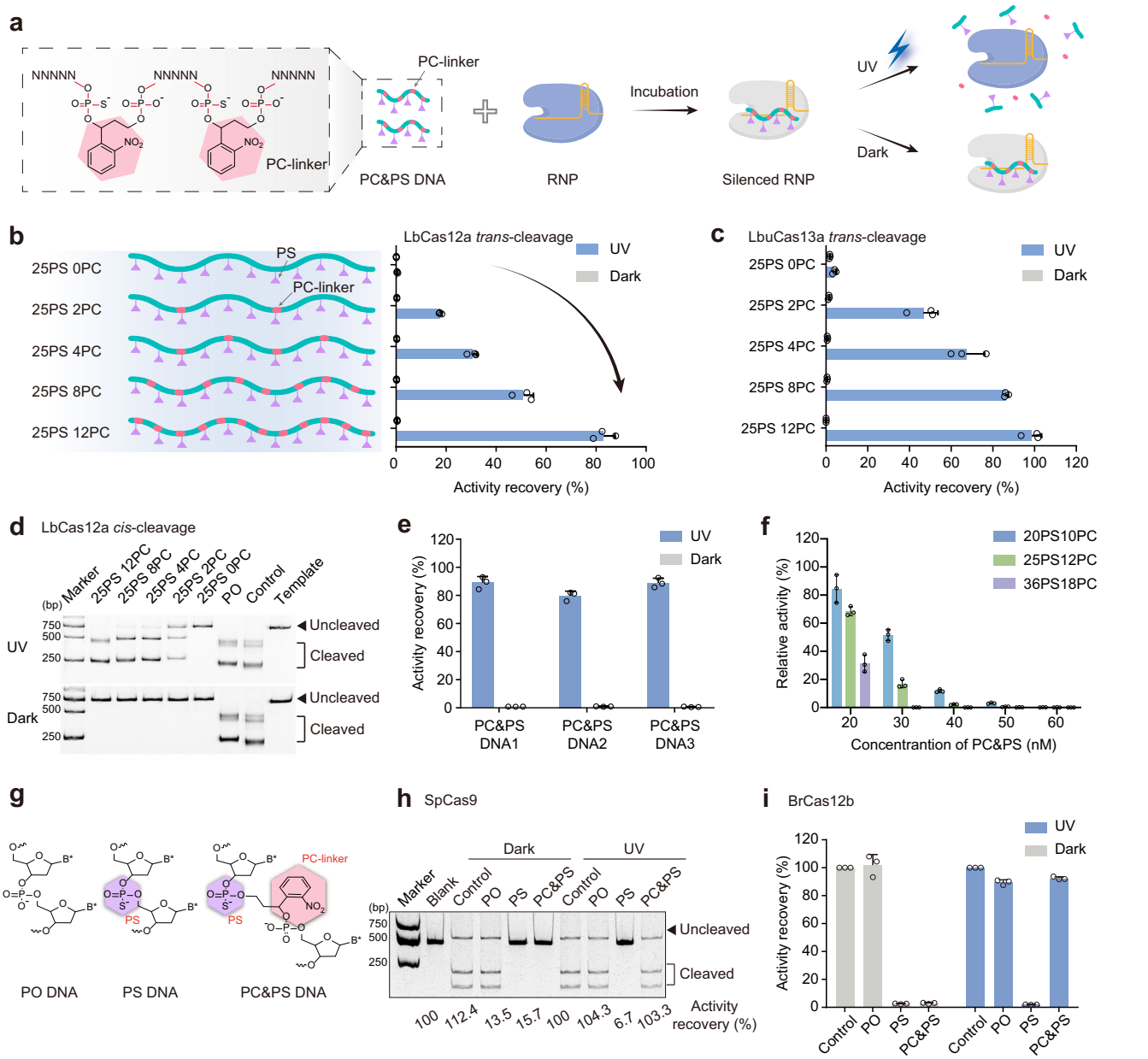



**Fig. 2 | In vitro development of the DNACas strategy. a** Schematic diagram illustrating the modulation of LbCas12a system activity by photoregulation of PC&PS DNA. **b**–**d** Measurement of the light-switching behavior of PC&PS DNA (random base composition, 26 nt in length) embedded with different amounts of PC-linker against *trans*-cleavage of LbCas12a (**b**) and LbuCas13a (**c**), and *cis*-cleavage of LbCas12a (**d**). **e** Measurement of the light-switching behavior of three PC&PS DNAs against LbCas12a. PC&PS DNA1, PC&PS DNA2, and PC&PS DNA3 have the same length (21 bases with 20 PS modifications) and are embedded with the same number of PC-linkers (10 PC-linkers) with different base compositions. **f** Evaluation of the concentration-dependent inhibitory effects of LbCas12a by three PC&PS DNAs (20PS10PC, 25PS12PC, 36PS18PC) with varying lengths. The experiment was conducted without UV light treatment. The final concentration of the LbCas12a is 15 nM. Relative activity is defined as the ratio of LbCas12a activity in the experimental group containing PC&PS DNA to that in the control group without PC&PS DNA. **g** The chemical structural formulas of PO DNA, PS DNA, and PC&PS DNA. **h**, **i** Evaluation of the photoregulatory ability of PO DNA, PS DNA, and PC&PS DNA on *cis*-cleavage activity of SpCas9 (**h**) and *trans*-cleavage activity of BrCas12b (**i**). The activity recovery was calculated by comparison to the native Cas protein for cleaving the same target. The long linear dsDNA containing the putative on-target sequence was cleaved by the Cas9 protein complexed with single-guide RNA (sgRNA), resulting in two shorter dsDNA fragments. The cleavage rate in (**h**) was determined using ImageJ software by measuring the gray-values of the uncleaved band and calculating its relative ratio to the blank (representing blank control containing only the template DNA). The total length of the DNA sequences is equal to the number of PS modifications plus one. These DNA sequences and RNP were preincubated at room temperature for 5 min. In all experiments, UV represents UV (365 nm) light irradiation for 1 min. Data are represented as mean ± standard error ($n = 3$ technical replicates). Source data are provided as a Source Data file.

Having demonstrated the light regulation of LbCas12a and LbuCas12a activity with DNACas, we next examined whether this strategy is also applicable to other CRISPR–Cas systems. Therefore, we compared the regulatory capacity of PO DNA, PS DNA, and PC&PS DNA in parallel (Fig. 2g). As expected, both PC&PS DNA and PS DNA effectively inhibited the *cis*-cleavage activity of SpCas9, but only the PC&PS DNA could restore enzyme activity upon light exposure. In contrast, PO DNA neither inhibited SpCas9 activity nor exhibited light-responsive properties (Fig. 2h). It is also observed that PC&PS DNA mediated similar light regulation efficiency in the BrCas12b[46] system, suggesting that DNACas represents a universal strategy for regulating CRISPR–Cas system activity (Fig. 2i).

https://doi.org/10.1038/s41467-025-61094-5

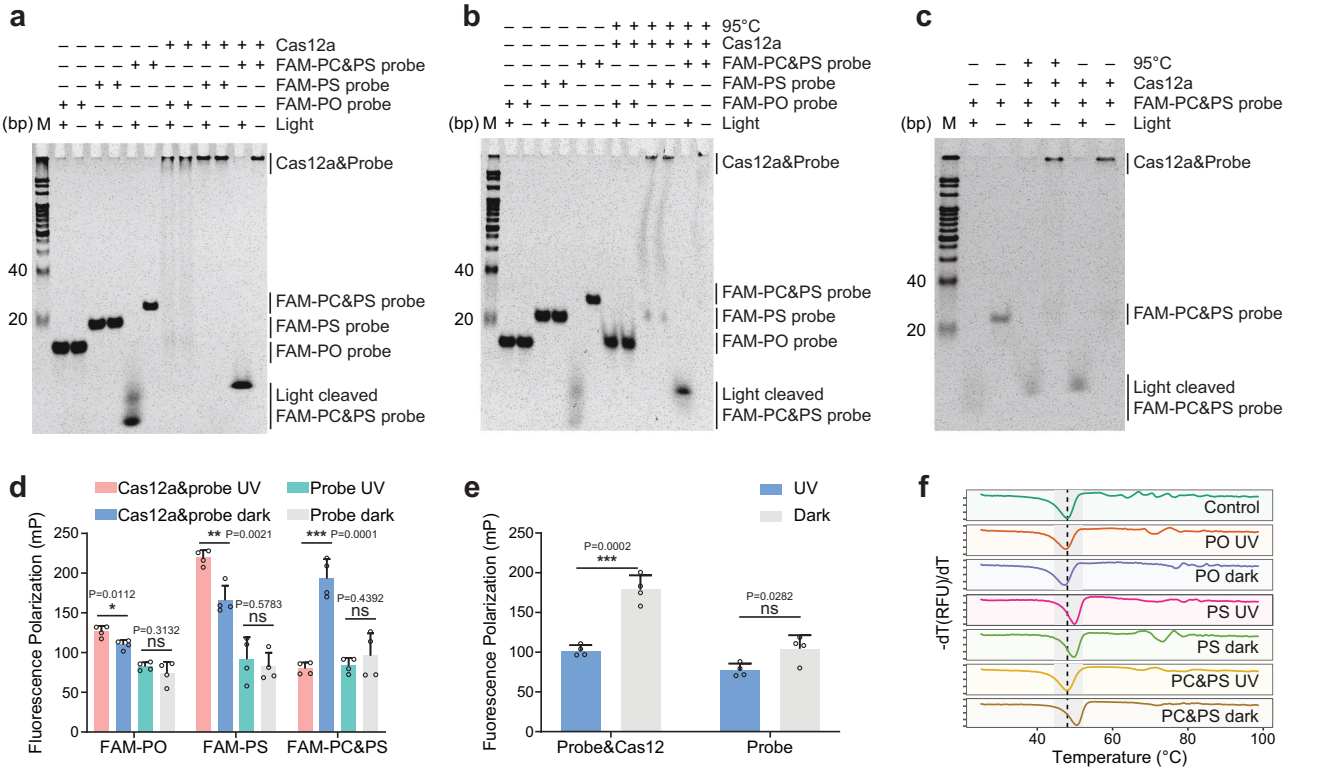



**Fig. 3 | Experimental observation of the working mechanism of DNACas.** **a**, **b** FAM terminal-labeled PO probe, PS probe, and PC&PS probe were incubated at room temperature (**a**) and 95 °C (**b**) with LbCas12a and subjected to polyacrylamide gel electrophoresis (PAGE) assay. DNA probes without incubation with Cas were also analyzed using electrophoresis as a control. **c** These analyses are identical to those shown in (**a**, **b**), except that the probe used is FAM mid-labeled PC&PS probe. **d** FAM terminal-labeled PO probe, PS probe, and PC&PS probe were incubated with LbCas12a and subjected to fluorescence polarization analysis. **e** Theses analyses are identical to those shown in (**d**), except that the probe used is a FAM mid-labeled PC&PS probe. The experiment results of fluorescence polarization were presented as mean ± standard error ($n = 4$ technical replicates). **f** PTS assay was employed to determine the melting curve of LbCas12a incubated with PO DNA1, PS DNA1, and PC&PS DNA1. In all experiments, UV represents 365 nm light irradiation for 1 min. *P* value was determined using an unpaired Student's t-test. $^{***}p < 0.001$, $^{**}p < 0.01$, $^{*}p < 0.05$, ns-not significant ($p > 0.05$). 'M' stands for marker. Source data are provided as a Source Data file.

## Working mechanism of DNACas

In the DNACas experiments, incubation of PS DNA or PC&PS DNA with LbCas12a sufficiently silenced enzyme activity, indicating that both PS DNA and PC&PS DNA bind to LbCas12a with high affinity. To assess the working mechanism of PC&PS DNA-mediated regulation of LbCas12a activity, we used an electrophoretic migration assay to evaluate the binding behavior of fluorescein amidite (FAM) terminal-labeled single-stranded PO, PS, and PC&PS probes with LbCas12a. As shown in Fig. 3a, the PO probe exhibited weak and incomplete binding to LbCas12a at room temperature, whereas the PS probe was firmly bound to LbCas12a, unaffected by light irradiation. The PC&PS probe binds to LbCas12a similarly to the PS probe, but its binding band disappears after light irradiation, with a smaller dye band appearing, indicating that the fragmented PC&PS probe separates from LbCas12a (Fig. 3a).

To test the binding stability, the above three binding products were heat-treated at 95 °C and subjected to an electrophoretic migration assay. The results showed that the binding of PO probe to the LbCas12a enzyme was thermally unstable, while the binding of the PS probe and PC&PS probe to LbCas12a exhibited higher thermal stability (Fig. 3b). And the dissociation occurred only after light irradiation with the PC&PS probe (Fig. 3b). To rule out the possibility that the PC&PS probe was not completely detached from the LbCas12a protein, we further tested the binding behavior using FAM mid-labeled PC&PS probe, in which the FAM group is conjugated at the central position of the probe. If only partial dissociation occurs, the FAM mid-labeled probe could still bind to LbCas12a. As shown in Fig. 3c, similar dissociation behavior was observed after light irradiation regardless of incubation at room temperature or 95 °C, indicating that the dissociation was complete. Considering that the binding behavior may change during electrophoresis, we used fluorescence polarization to observe this binding and dissociation. In this assay, an increase in fluorescence polarization values indicates probe binding, while a decrease suggests dissociation. Using the same FAM terminal- and mid-labeled probes, we observed binding and dissociation behaviors similar to those in the electrophoretic migration assay (Fig. 3d, e). Thus, it can be concluded that light cleavage-mediated dissociation of the PC&PS probe from the enzyme is the fundamental work mechanism for DNACas.

We next investigated whether PC&PS DNA binding induced a conformational change in LbCas12a. To evaluate the conformational effects, we used the protein thermostability shift (PTS) assay, which detects changes in the folded/unfolded state of the protein by using a hydrophobic binding dye to identify the exposure of the hydrophobic region during temperature ramping[47]. As shown in Fig. 3f, identical $T_m$ peaks were obtained for naked LbCas12a and LbCas12a samples incubated with PO DNA. Binding of PS DNA or PC&PS DNA caused an increase of approximately 3°C in the $T_m$. After light irradiation, LbCas12a labeled with the PO DNA and PS DNA groups maintained their original $T_m$ peaks, while the PC&PS DNA group recovered the native LbCas12a $T_m$ peaks. These results suggest that PS-mediated affinity stabilizes but does not destroy the conformation of LbCas12a (Fig. 3f), whereas light-mediated dissociation restores the normal conformation of LbCas12a.

## Structural basis of DNACas

We used LbCas12a as a model protein to further elucidate the working mechanism of DNACas at near-atomic resolution. The LbCas12a

protein in complex with PC&PS DNA and crRNA was subjected to a standard cryo-electron microscopy (cryo-EM) workflow (Supplementary Tab. 1). After data processing, most particles resulted in a distinct map with an extra density in the target DNA binding site compared to the crystal structure of LbCas12a-crRNA complex (PDB: 5ID6) (Supplementary Figs. 3, 5). We suspect that the extra density represents the PC&PS DNA (Fig. 4). To confirm that, we treated the LbCas12a-crRNA-PC&PS DNA with UV irradiation and solved the cryo-EM structure using the same method. Interestingly, the map resulting from most particles is almost identical to the architecture of the LbCas12a-crRNA complex (PDB: 5ID6) (Supplementary Figs. 4, 6) without any extra densities. Therefore, the extra density located in the target DNA binding site of LbCas12a is supposed to be the PC&PS DNA, which disappeared after PC&PS DNA digestion by UV irradiation.

To explore the structure deformation detail upon PC&PS DNA binding, the molecular models of LbCas12a-crRNA and LbCas12a-crRNA-PC&PS DNA were solved. The crRNA consists of the 21-nt repeat region (U(+21)-U(+1)) and 20-nt spacer region (G(1)-A(20)). For LbCas12a: crRNA, the nucleotides A(+20)-U(5) in the crRNA can be modeled, while no electron density was observed for the nucleotides U(6)-A(20) in the crRNA, suggesting that these regions are flexible and disordered in the cryo-EM structure. For LbCas12a: crRNA: PC&PS DNA complex, only the nucleotides A(+20)-U(7) in the crRNA and six modified nucleotides in the PC&PS DNA can be modeled. Interestingly, the sequence-independent PC&PS DNA not only occupies the target DNA binding site but also partially binds to the nucleotides G(3) to U(7) in the crRNA spacer region (Fig. 4). Considering that four PC&PS DNAs composed of homopolymeric sequences effectively regulate the activity of LbCas12a in Supplementary Fig. 1, we speculate that the partial binding between crRNA and PC&PS DNA occurs randomly. The occupation of the target DNA binding of crRNA by PC&PS DNA serves as the primary mechanism for regulating the activity of the LbCas12 protein. Structural comparison between LbCas12a-crRNA-PC&PS DNA and LbCas12a-crRNA indicates that PC&PS DNA stabilized the PI (protospacer adjacent motif (PAM)-interacting) domain and moved upward the REC (recognition) lobe slightly, which allows the PC&PS DNA to occupy the target DNA binding pocket and spatially complement the crRNA (Supplementary Fig. 7a). Meanwhile, the PC&PS DNA can occupy the target DNA binding site with the inhibition effect on the LbCas12a compared to the activation effect of target DNA (Supplementary Fig. 7b). After UV treatment, the vastly decreased ratio of the PC&PS DNA-containing particles suggested that the UV irradiation degraded the PC&PS DNA and released its fragments. These structural studies indicate that the UV-sensitive PC&PS DNA occupies the target DNA binding site and reshapes the LbCas12a through the PI domain and REC lobe, which may block the binding of DNA target. Under UV irradiation, PC&PS DNA is degraded and released from the target DNA binding pocket.

### DNACas boosting light-controlled one-pot LAMP-BrCas12b assay development

We envision that DNACas could be employed to improve light-controlled CRISPR-based nucleic acid detection. In the conventional CRISPR-based one-pot assay, the cleavage activity of the CRISPR system leads to the degradation of the amplification substrate, which results in the inefficiency of the one-pot assay[48,49]. Therefore, there is a need to develop methods to control the activity of the CRISPR system to facilitate the development of simpler and more sensitive CRISPR diagnostics. Previously, we and others have developed photocontrolled CRISPR assay through light regulation of gRNA activity[7–9]. However, these assays require redesigning and optimizing the protective oligo or the caged crRNA for different targets. In addition, the modified gRNAs used in these approaches rely heavily on chemical synthesis, limiting their applicability to other long-stranded gRNAs that are difficult to synthesize chemically, such as those adapted to Cas12f or Cas12b systems. Unlike these methods, DNACas regulates the Cas protein rather than the gRNA, exhibiting the potential for developing a universal photocontrolled CRISPR assay.

Considering that LAMP is more economically efficient than recombinase polymerase amplification (RPA), we evaluated the feasibility of developing a light-controlled one-pot LAMP-BrCas12b assay (light-controlled one-pot assay) because BrCas12b and LAMP have compatible working temperatures. With this system, LAMP amplification will not be affected by BrCas12b cleavage. Upon completion of the LAMP reaction, BrCas12b detection was initiated by light irradiation (Fig. 5a), triggering BrCas12b's *cis*-cleavage to recognize and cleave the LAMP amplicons. This simultaneously activates its *trans*-cleavage activity, which non-specifically cleaves the FQT12 probe in the reaction system, generating fluorescent signals. The results confirmed that the light-controlled one-pot assay significantly improved the detection efficiency. As demonstrated, a plasmid DNA containing the severe acute respiratory syndrome coronavirus 2 (SARS-CoV-2) *nucleocapsid* (*N*)-gene, undetectable by the conventional one-pot BrCas12b-LAMP assay, was successfully detected by light-controlled one-pot assay with a high signal-to-noise ratio (Fig. 5b, Supplementary Data 2). Further detailed target concentration detection experiments showed that the sensitivity of the light-controlled one-pot assay was 3 orders of magnitude higher than the conventional one-pot assay (Fig. 5c). Furthermore, the light-controlled one-pot assay has shown favorable specificity (Fig. 5d).

To validate the effectiveness of the light-controlled one-pot assay for detecting clinical samples, we performed it to detect suspected clinical samples of SARS-CoV-2. Given that SARS-CoV-2 is an RNA virus, an additional reverse transcription step was first introduced to convert RNA into complementary DNA (cDNA) for subsequent detection. A cycle threshold ($C_t$) value of 38 was set as the criterion for positive samples. The results of the light-controlled one-pot assay closely matched those obtained from a parallel reverse transcription quantitative PCR (RT-qPCR) analysis using a clinically approved kit, except two PCR-confirmed positive samples ($C_t$ >37) that were not detected (Fig. 5e, Supplementary Fig. 8, and Supplementary Tab. 2). It is worth noting that samples with $C_t$ > 35 are generally considered to have lower infectivity, indicating that the method proposed in this study is sufficient for clinical testing. The receiver operating characteristics (ROC) curves for the light-controlled one-pot assay demonstrated an area under the curve (AUC) of 0.9963 for the N gene (Fig. 5f). And the sensitivity and specificity of the proposed method in this study compared to the RT-qPCR method were 97.0% and 100%, respectively (Fig. 5g). These findings highlight the reliability and clinical applicability of the light-controlled one-pot assay.

Furthermore, we performed the method to detect Epstein-Barr virus (EBV) suspected clinical samples (Fig. 5h). EBV is a member of the herpesvirus family, which is widespread in the population and persists throughout a person's lifetime. EBV infections may induce a variety of cancers, such as lymphoma, nasopharyngeal carcinoma, gastric carcinoma, and others[50–53]. Therefore, EBV can be a biomarker for screening of these diseases. In this study, we first designed three sgRNAs for the EBV and evaluated their activities in the light-controlled one-pot assay (Supplementary Fig. 9, Supplementary Data 2). SgRNA3 was selected for use in subsequent experiments due to its high reaction rate. Then, we collected and extracted nucleic acids from 23 clinical blood samples. According to the results of the qPCR method, there were 17 positive samples and 6 negative samples (Supplementary Fig. 10). These samples were then analyzed under the above-optimized conditions using the light-controlled one-pot assay. As shown in Fig. 5i, the detection results of the light-controlled one-pot assay were consistent with qPCR for all samples except sample 14 ($C_t$ value 37.72).

https://doi.org/10.1038/s41467-025-61094-5

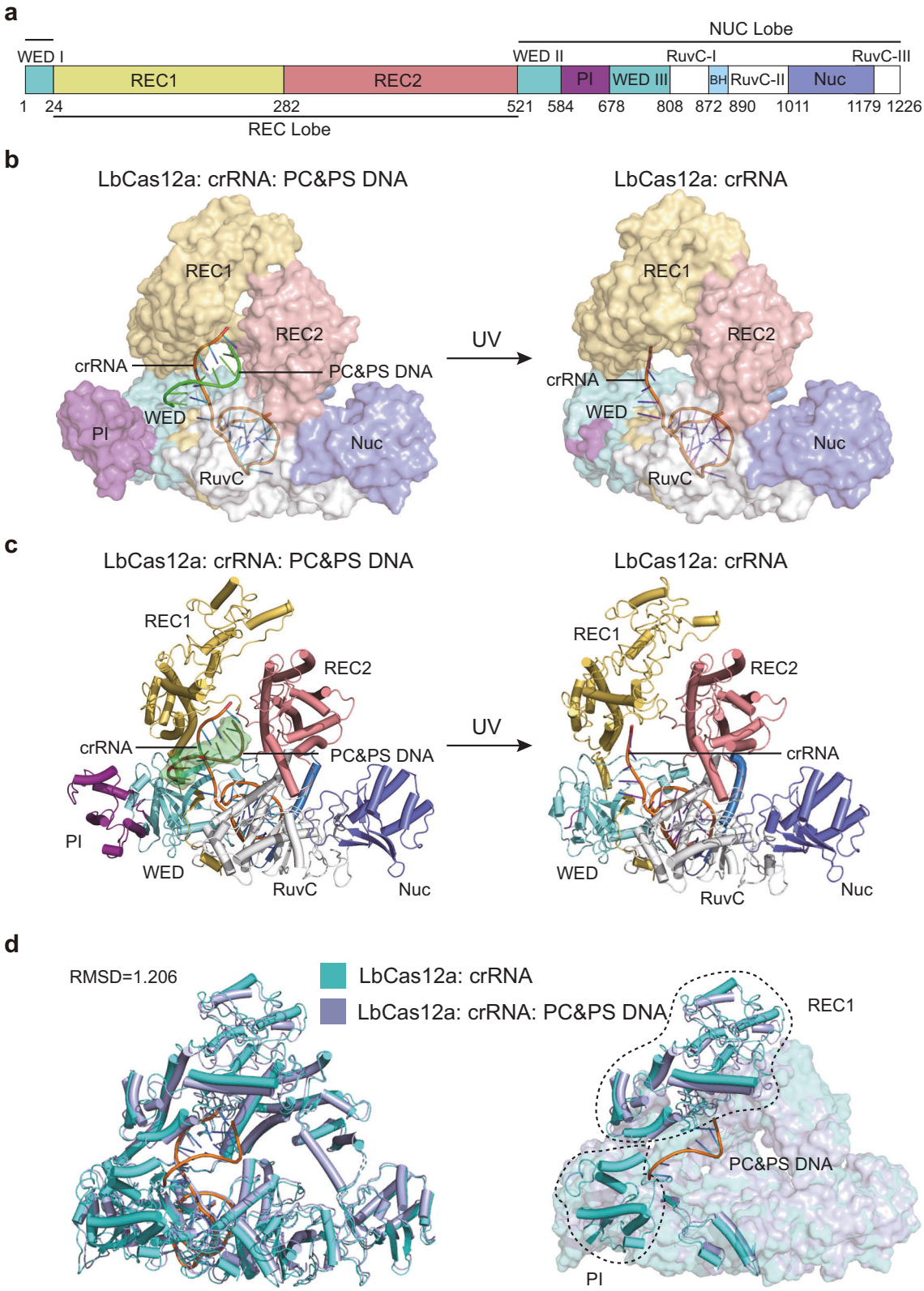



**Fig. 4 | Overall structure of the LbCas12a-crRNA-PC&PS DNA complex with or without light irradiation. a** Schematic diagram of the domain organization of LbCas12a. REC recognition, PI protospacer adjacent motif (PAM) interacting, WED wedge, BH bridge helix, Nuc nuclease. **b** Surface representations of LbCas12a-crRNA-PC&PS DNA complex with or without light irradiation. Individual LbCas12a domains are colored according to the scheme in (**a**). crRNA and PC&PS DNA in cartoon are colored orange and green, respectively. **c** Overall structure of the LbCas12a-crRNA-PC&PS DNA complex with or without light irradiation. The surface of PC&PS DNA is shown and colored green. **d** Superimposed cartoon models of LbCas12a-crRNA-PC&PS DNA and LbCas12a-crRNA are shown on the left. The RMSD is around 1.026. The structural difference between LbCas12a-crRNA-PC&PS DNA and LbCas12a-crRNA is highlighted on the right. The primary conformational deformation in REC1 and PI domain is labeled with dashed lines. crRNA and PC&PS DNA in the cartoon are colored orange.

https://doi.org/10.1038/s41467-025-61094-5

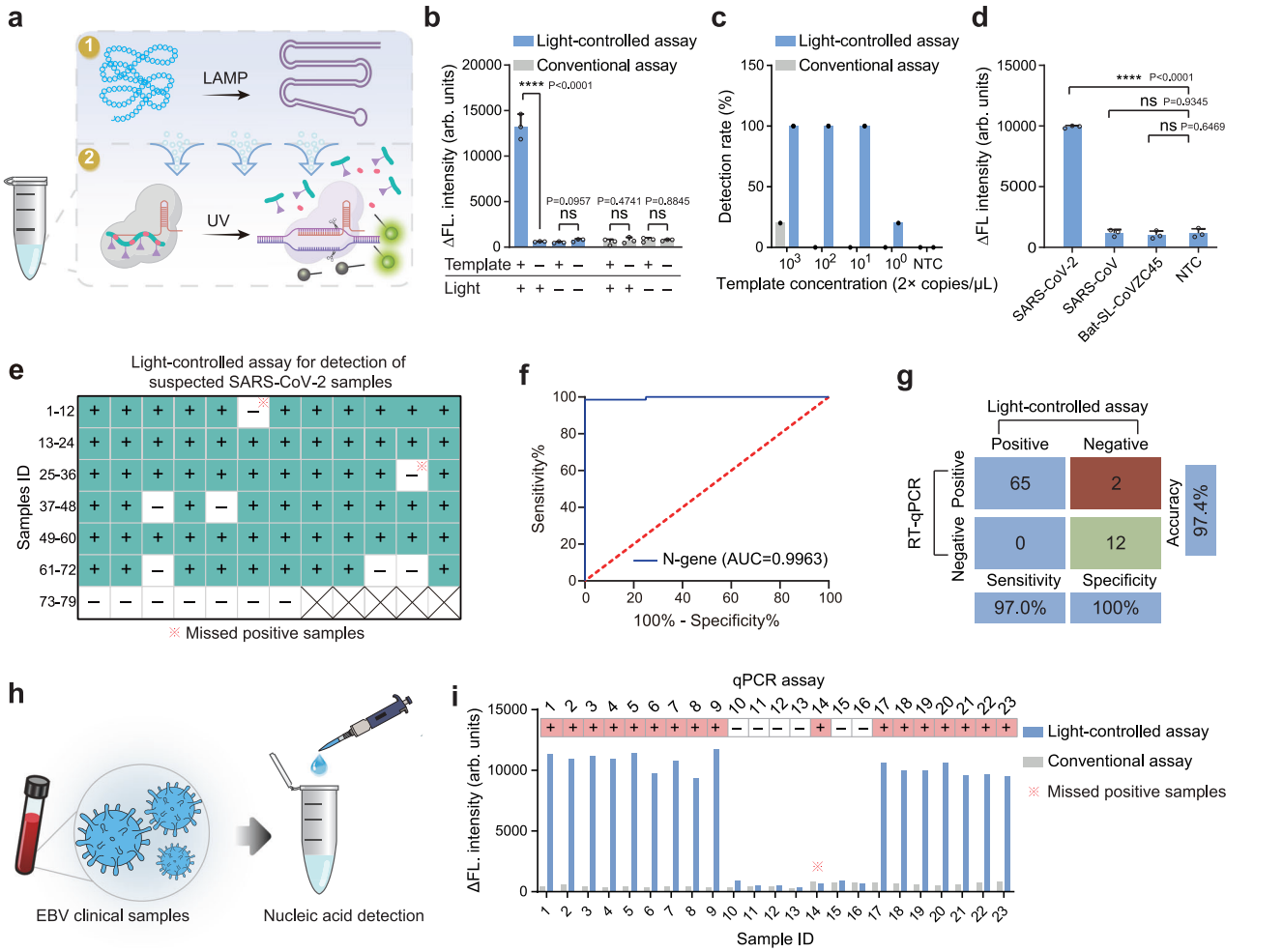



**Fig. 5 | Application of DNACas to develop light-controlled one-pot assay for in vitro nucleic acid detection. a** Schematic diagram of the light-controlled one-pot assay. For the light-controlled one-pot assay, BrCas12b is temporarily silenced and can be rapidly activated by light irradiation once the LAMP reaction is complete. This assay has high detection efficiency because the LAMP reaction is not affected by BrCas12b cleavage. **b** Detection of plasmid DNA (SARS-CoV-2 *N*-gene, 200 copies/μL) template by light-controlled one-pot assay and the conventional one-pot assay. Data are represented as mean ± standard error ($n = 3$ technical replicates). **c**, Detection of plasmid DNA (SARS-CoV-2 *N*-gene) template with gradient dilution by light-controlled one-pot assay and the conventional one-pot assay. The detection rate represents the rates of the positive over five experiments. **d** Specificity of the light-controlled one-pot assay in analyzing *N*-gene plasmid DNA of SARS-CoV-2 against other coronaviruses (severe acute respiratory syndrome coronavirus (SARS-CoV) and bat SARS-like coronavirus (bat-SL-CoVZC45)). Data are represented as mean ± standard error ($n = 3$ technical replicates). **e** Detection of 79 clinical SARS-CoV-2 RNA samples by light-controlled one-pot assay. **f** ROC curve analysis of the detection accuracy in the clinical application of the light-controlled one-pot assay. **g** Matrix summarizing the assay discrimination performance between positive and negative clinical samples using the light-controlled one-pot assay and RT-qPCR. **h** Schematic illustrating the light-controlled one-pot assay for detecting EBV-suspected clinical samples. **i** 23 EBV-suspected clinical samples were confirmed by light-controlled one-pot assay and qPCR method. The bar graph shows the fluorescence detection results of the light-controlled one-pot assay. "+" represents the positive sample identified by light-controlled one-pot assay or qPCR, and "–" represents the negative sample identified by light-controlled one-pot assay or qPCR. Samples marked with a red ※ are positive samples that were missed by the light-controlled one-pot assay. ΔFL. Intensity represents the difference between the 90 min and initial fluorescence value. *P*-value was determined using an unpaired Student's t-test. ****$p < 0.0001$, ns-not significant ($p > 0.05$). Source data are provided as a Source Data file.

## DNACas mediated development of in vivo spatiotemporally gene editing strategy

The CRISPR–Cas9 system, an RNA-guided DNA endonuclease, has been widely used in gene editing[2,5]. Given the irreversible nature of gene editing, the ability to target only a subset of cells at specific times would significantly enhance the CRISPR–Cas system's precision. Conditional gene editing could minimize off-target effects by restricting the CRISPR–Cas system's activity to designated cells. Several efforts have focused on making the CRISPR–Cas system light-responsive to allow precise temporal control over gene editing or expression. These optogenetic strategies include using light-responsive Cas9 proteins or gRNAs[10,11,13,14]. However, challenges remain, including unintended activity in the dark, incomplete restoration of Cas9 function, and the need to design photo-responsive gRNA for different target sites.

In this study, we microinjected the PC&PS DNA/RNP complex (composed of Cas9 and sgRNA) targeting the tyrosinase (*tyr*) gene[54], into the one-cell stage of zebrafish embryos, preventing RNP from recognizing the target genomic DNA sequence until brief illumination triggered light-induced gene editing, which resulted in zebrafish exhibiting an albino phenotype (Fig. 6a). The spatiotemporal control ability of the 20PS10PC-coupled CRISPR–Cas9 system for gene editing in zebrafish was first evaluated. The initial results showed that 20PS10PC did not demonstrate effective spatiotemporal regulation of CRISPR–Cas9 activity in zebrafish (Supplementary Fig. 11). Subsequently, the inhibition of CRISPR–Cas system was optimized by

https://doi.org/10.1038/s41467-025-61094-5

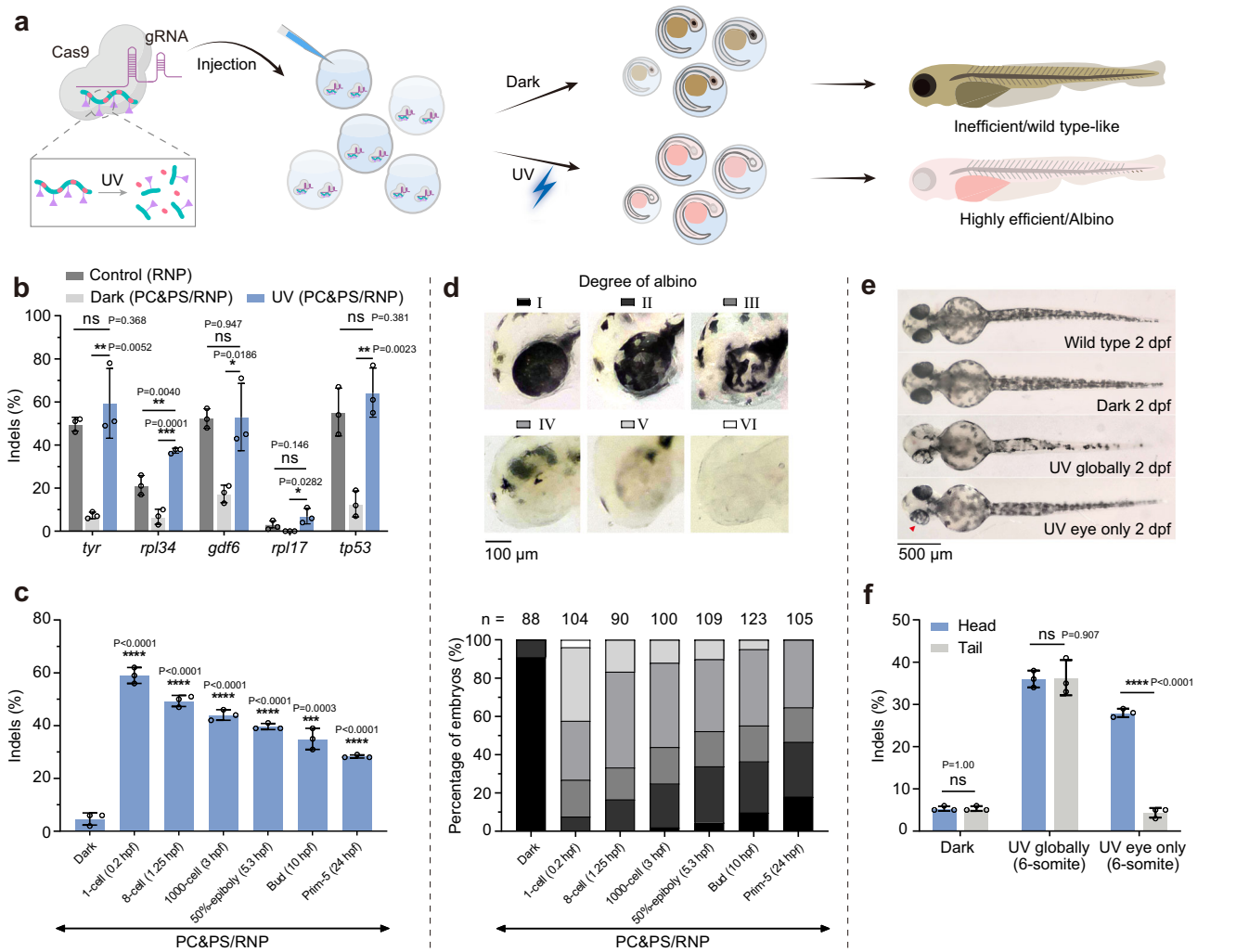



**Fig. 6 | Spatiotemporal gene editing in zebrafish. a** Schematic representation of light-regulated CRISPR–Cas9-mediated gene editing using DNACas in zebrafish. **b** Indel analysis through Sanger sequencing of PCR-amplified genomic DNA extracted from injected embryos. **c**, **d** Temporally resolved light-mediated gene editing in zebrafish embryos microinjected with PC&PS DNA and RNP, and globally exposed to 365 nm light at the indicated developmental stages. **c** shows the indel analysis of light-activated RNP at different development stages in zebrafish. **d** displays representative images of each knockout phenotype (upper panel). The total number of embryos displaying each knockout phenotype category is shown at the bottom of (**d**) for each treatment group ($n = 88$–$123$). **e** Representative images of zebrafish embryos microinjected with PC&PS DNA and RNP, either locally exposed to 405 nm laser light in the eye area at the 6-somite stage, globally irradiated with 365 nm light, or kept in the dark as a negative control. Untreated wild-type embryos served as a blank control. **f** Indel analysis of the head and tail regions of zebrafish treated as described in (**e**). Data are presented as mean ± standard error (n = 3 technical replicates); *P* value was determined using an unpaired Student's t-test. $^{****}p < 0.0001$, $^{***}p < 0.001$, $^{**}p < 0.01$, $^{*}p < 0.05$, ns-not significant ($p > 0.05$). hpf represents hours post-fertilization. Source data are provided as a Source Data file.

altering the distribution of PC-linkers in the sequences, increasing the number of PS modifications, or adding 2′-F modifications (Supplementary Fig. 12). The 2′-F modification, which involves replacing the hydrogen atom at the 2′ position of the ribose with a fluorine atom, has been reported to enhance the binding affinity of DNA to proteins[41,55]. As a result, 26PS8PC was selected for subsequent experiments. To further refine the reaction conditions, the amounts of PC&PS DNA and RNP in the reaction system (Supplementary Fig. 13) were optimized. The results showed the highest reaction efficiency was achieved with 12 fmol PC&PS DNA and 6 fmol RNP. Next, we characterized DNACas efficiency by targeting five endogenous loci and found that the light-activated experimental group exhibited comparable light-induced indel efficiency to the control group (Fig. 6b), suggesting that the RNP almost fully recovered its activity after light exposure. For temporally controlled gene editing, zebrafish embryos were microinjected with the PC&PS DNA/RNP complex at one cell stage and exposed to UV light irradiation at various developmental stages. Two days post-fertilization (dbf), the embryos were imaged and assessed for *tyr* gene mutations using an indel mutation analysis assay (Fig. 6c, d). As expected, embryos injected with PC&PS DNA/RNP showed no significant *tyr* gene mutations, either phenotypically or at the genomic DNA level, in the absence of light exposure. In contrast, UV light exposure induced *tyr* gene mutations and an albino-like phenotype in the injected embryos, with gene knockout efficiency decreasing as irradiation was delayed.

We then investigated the potential for spatially restricted gene editing in zebrafish using DNACas. Embryos were microinjected at the one-cell stage and kept in the dark until reaching the 6-somite stage, when the head and tail regions became visible. At this point, one eye of the embryo was selectively irradiated using a 405 nm laser in a confocal microscope[23]. Two days post-treatment, we observed melanin expression in the eye of the locally irradiated embryos (Fig. 6e). Additionally, we analyzed *tyr* gene mutations in the head and tail regions of the same embryos separately, detecting mutations only in

the head (Fig. 6f). In contrast, globally irradiated embryos displayed uniform mutations in both the head and tail, while embryos kept in the dark showed no detectable mutations, confirming the feasibility of localized gene editing using DNACas.

Moreover, to ensure that DNACas-mediated editing does not compromise embryonic development, we evaluated the toxicity of the system under various experimental conditions. Specifically, we quantified malformation and mortality rates in zebrafish embryos at 24 h post-fertilization (hpf). Embryos exposed to UV irradiation at different durations (0 s, 10 s, 30 s, 60 s) or PC&PS DNA embedding at increasing amounts (0 fmol, 2 fmol, 4 fmol) during the one-cell stage were analyzed. Notably, UV exposure ≤ 60 s and PC&PS DNA amounts ≤ 4 fmol exhibited mortality and malformation rates comparable to untreated controls (Supplementary Fig. 14a, b). To characterize treatment-induced transcriptional alterations, we conducted RNA-seq analysis on embryos following UV or PC&PS DNA interventions. Principal component analysis demonstrated substantial transcriptional similarity between UV-irradiated embryos and dark controls (Supplementary Fig. 14c). When applying the same analytical approach to PC&PS DNA-treated groups, we observed close clustering in principal component space among PC&PS DNA-treated embryos (both with and without UV exposure) and RNP-treated counterparts (Supplementary Fig. 14d). Under stringent experimental controls, neither UV irradiation nor PC&PS DNA treatment induced significant differential gene expression when applying thresholds of $|\log_2(\text{fold change})| > 1$ with adjusted $p < 0.001$ (Supplementary Fig. 14e, f). Considering the balance between DNACas efficiency, UV-induced cellular damage, and PC&PS DNA toxicity, we optimized experimental parameters by marginally compromising efficiency to minimize adverse effects (Supplementary Fig. 14g).

In conclusion, we developed a photoswitchable CRISPR–Cas9 gene editing system based on DNACas. This approach utilizes the addition of PC&PS DNA to the reaction system, eliminating the need to modify the regulatory strategy for different target sites, allowing precise spatiotemporal control of gene editing in vivo, and can be easily extended to gene regulation of other newly discovered Cas proteins.

## Discussion

PS DNA is chemically modified nucleic acids obtained by replacing a nonbridging oxygen atom with sulfur and has been widely used in nucleic acid therapy[36]. Recently, PS DNA has been recognized for its broad protein-binding affinity[38–40,56]. This binding affinity also leads to extensive inhibition of protein function, resulting in cytotoxicity. In this study, we determined that PS DNA universally inhibits CRISPR–Cas activity. What is particularly interesting is that this inhibitory effect depends on the number of PS modifications on PS DNA. We note that such a PS DNA-dependent inhibition phenomenon was also reported 30 years ago[57]. Although PS DNA has been recognized as a protein activity inhibitor for a long time, further development of this mechanism into an enzyme activity regulation strategy has not been reported. Based on this mechanism, we proposed a simple DNACas strategy and focused on its application in advancing CRISPR technology. Compared with conventional photoregulation methods, DNACas has some revolutionary methodological features, including the elimination of the need for protein engineering modification with photocaged groups, simple and universal use, and excellent light-switching efficiency (Supplementary Tab. 3).

We first used LbCas12a as a model to understand how DNACas works. PS DNA is known to be more hydrophobic than PO DNA[56]. Employing the BLI and PTS assays, we demonstrated that PS DNA exhibits a higher binding affinity for LbCas12a, and their interaction promotes the formation of a more stable protein conformation. Additionally, electrophoretic migration and fluorescence polarization assays confirmed that PC&PS DNA fragments were detached from LbCas12a after light irradiation. PTS experiments also confirmed that LbCas12a could return to its native conformation after light-mediated PC&PS DNA breakage. Cryo-EM provided further insights into the regulatory mechanism of PC&PS DNA on CRISPR–Cas system activity. After interacting with the RNP, PC&PS DNA occupies the target DNA binding pocket, thereby silencing the activity of the Cas protein. Overall, these crucial experiments elucidate the mechanism by which enzyme activity can be significantly restored upon light irradiation. Notably, DNACas successfully achieved optical control over four tested CRISPR–Cas enzymes (LbCas12a, BrCas12b, LbuCas13a, SpCas9) using the same PC&PS DNA sequence, highlighting its simplicity and generality. It is also worth noting that although PC&PS DNA was employed in the current study, we demonstrated that single-stranded RNA with designed PC&PS modifications were also effective (Supplementary Fig. 15). In addition, although we primarily focused on the regulation of CRISPR–Cas activity in this study, DNACas can also be applied to the photoregulation of other proteins, such as T7 RNA polymerase, RNase A, and restriction endonuclease (Nde I), due to the extensive protein-binding properties of PS DNA[58] (Supplementary Fig. 16).

DNACas exhibits light-switching efficiency. This flexible light response capability drove us to develop nucleic acid detection assays. In the light-controlled one-pot LAMP-BrCas12b detection method, its sensitivity for nucleic acid detection is improved by approximately 3 orders of magnitude compared to the conventional one-pot method. Moreover, compared with our previously developed CRISPR detection technology involving the photocontrol of crRNA activity[7,8], the currently developed light-controlled one-pot LAMP-CRISPR strategy has versatility because the Cas protein activity is controlled directly. This method is convenient and cost-effective since the same PC&PS DNA can be adapted to detect different target nucleic acids. We further demonstrate that DNACas also has the potential to facilitate the development of quantitative nucleic acid detection assay. In the conventional CRISPR–Cas systems, the activation is disorganized and uncontrolled, which significantly affects its accuracy in nucleic acid quantification applications (Supplementary Fig. 17). In contrast, DNACas offers light-dependent activation, providing precise temporal and spatial control. Therefore, the DNACas was introduced to develop a light-controlled CRISPR–Cas assay (light-controlled assay) to address the problem of disordered reactions present in the conventional assay (Supplementary Fig. 17). In this system, the CRISPR–Cas system remains silent until exposed to UV illumination, rendering it highly controllable in terms of timing. Moreover, the presence of PC&PS DNA does not adversely affect the detection sensitivity of the CRISPR–Cas system and is expected to enhance its quantitative detection capabilities (Supplementary Figs. 17, 18).

DNACas also demonstrated its superiority in advancing a spatiotemporal gene editing strategy. The method is straightforward and versatile that effectively overcomes two key limitations of conventional methods based on photo-regulated gRNA and Cas protein: insufficient recovery of Cas protein activity and the need for customized gRNA designs for different target sites.

Although this study has thoroughly validated the DNACas strategy for advancing molecular diagnostics and spatiotemporal control of gene editing, several limitations remain that require attention. The cleavage of PC&PS DNA depends on UV irradiation, which can cause potential adverse biological effects, such as dsDNA breaks, tissue damage, and even apoptosis or necrosis. While RNA-seq analyses confirmed no significant differences with UV exposure durations of less than 60 s (Supplementary Fig. 14), these assessments focused primarily on short-term responses and did not address potential chronic toxicity or genetic risks associated with the long-term in vivo persistence of molecules like PC-linkers and PS modifications.

Additionally, the effectiveness of DNACas has been validated only in the zebrafish model, and its applicability in other biological systems,

such as mammals and plants, remains to be further explored. Given the limited tissue penetration of UV light, the activation efficiency of DNACas in higher organisms may be constrained. Thus, the future development of light-sensitive molecules responsive to longer wavelengths, which could replace the current PC-linker in our system, may facilitate the application of this strategy in deep tissues. Moreover, in the DNACas system, the PC-linker regulates the cleavage of PC&PS DNA, reducing its binding affinity to proteins and enabling light-controlled release of protein activity. However, such regulatory effects are not necessarily confined to light-responsive mechanisms; alternative methods, such as chemically induced or enzymatically triggered cleavage, could also be explored to achieve efficient and precise control over PS DNA breakage.

The broad binding affinity of PC&PS DNA enhances its versatility for Cas proteins but also introduces several challenges. In complex reaction systems, PC&PS DNA may nonspecifically interact with various proteins. For example, DNACas requires an excess amount of PC&PS DNA to ensure reaction efficiency. The presence of free PC&PS DNA molecules may lead to unintended modulation of non-target proteins, reducing system specificity and limiting its applicability in more complex biological environments. Although no significant cytotoxicity was observed under low-dose conditions (≤4 fmol) (Supplementary Fig. 14), and the photoactivation process cleaves PC&PS DNA into small nucleotide fragments that substantially diminish its protein-binding capacity, the presence of excess PC&PS DNA prior to light activation may still impact the cellular or tissue microenvironment.

The regulation of protein activity by PC&PS DNA relies primarily on the PC-linker to control the breaking of its chemical bonds, enabling the "on-off" switching of protein activity. This mechanism provides a powerful tool for spatiotemporal control of protein activity. However, in biological systems, particularly in gene editing applications, regulating the "off-on-off" switching of protein activity would be of greater practical value. For instance, in gene therapy, precisely controlling the activation time window of the CRISPR–Cas system and promptly shutting down its activity after the reaction is completed would be crucial to minimizing off-target effects caused by prolonged activity. To achieve this, an effective strategy could involve introducing a photosensitive molecule responsive to a different wavelength of light into the gRNA: in the absence of light, the gRNA would normally guide Cas proteins to exert activity; however, under specific wavelength light, the photosensitive molecule would break, leading to the cleavage of the gRNA strand and rapidly deactivating the CRISPR system[21]. By combining this strategy with the DNACas strategy developed in this study, Cas protein activity could initially be shut down using PC&PS DNA. UV light would then degrade the PC&PS DNA, releasing the inhibition of Cas protein activity and initiating gene editing. Once the gene editing is complete, the light of another wavelength would be applied to cleave the photosensitive molecule on the gRNA, quickly shutting down CRISPR activity.

In conclusion, we demonstrated the simplicity and versatility of DNACas and leveraged its capabilities to advance in vitro and in vivo CRISPR techniques. The PC&PS DNA used in this study can be synthesized commercially, making it readily available to other laboratories. We anticipate that DNACas can be a powerful tool for developing other biotechnologies.

## Methods

### Ethics statement

The clinical SARS-CoV-2 samples were collected from patients with suspected SARS-CoV-2 infection who presented symptoms at Hubei Provincial Center for Disease Control and Prevention. The clinical trial on SARS-CoV-2 samples in this study has received formal approval from the ethics committee of the Hubei Provincial Center for Disease Control and Prevention/Academy of Preventive Medicine (2020-061-01). The clinical EBV samples were collected from patients with suspected EBV infection who presented symptoms at Sun Yat-sen University Cancer Center. The clinical trial on EBV samples in this study has received formal approval from the ethics committee of the Sun Yat-sen University Cancer Center (B2022-769-01). To ensure the protection of patient privacy, waivers of informed consent were approved by the ethics committee. This study involves the detection of EBV and SARS-CoV-2 nucleic acids in human clinical samples. No sex or gender information was collected or used, and the assays were not designed to evaluate sex-based differences. Therefore, sex and gender analyses are not applicable. All zebrafish experiments were approved by the University Animal Care and Use Committee of South China Normal University (SCNU-SLS-2023-022).

### Synthesis of DNA sequences for modulating CRISPR–Cas activity

All phosphorothioate DNA (PS DNA), phosphodiester DNA (PO DNA), and photocleavable phosphorothioate DNA (PC&PS DNA) were chemically synthesized and commercially obtained from Hippo Bio (Huzhou, China). These sequences were synthesized using a standard solid-phase synthesis method and purified by high-performance liquid chromatography (HPLC). Detailed information on these sequences is provided in the Supplementary Data and Supplementary Tables.

### PS DNA-mediated in vitro LbCas12a activity inhibition assay

PS DNAs or the PO-1 DNA, as listed in Supplementary Data 1, were used to evaluate the inhibitory effect on the LbCas12a *trans*-cleavage activity based on a fluorescent assay. The detailed experimental procedures are shown below. First, the PS DNA or PO-1 DNA was incubated with the pre-assembled LbCas12a (Bio-Lifesci, Guangzhou, China, catalog number: M20301-0500) and crRNA at room temperature for 5 min. Then, a mixture with a final concentration of 15 nM LbCas12a, 15 nM crRNA, 400 nM FQC6 probe, 100 pM dsDNA target, and PS DNA or the PO-1 DNA (100 nM for Fig. 1b, 60 nM for Fig. 1d) in 1 × LbCas12a reaction buffer was prepared, and the volume was adjusted to 20 μL with RNase-free water (TaKaRa, catalog number: 9012). The 1 × LbCas12a reaction buffer was composed of 5 mM Tris-HCl (pH9.0), 15 mM $MgCl_2$, 10 mM NaCl, 0.01% IGEPAL CA-630 (v/v) (Sigma-Aldrich, catalog number: 9002-93-1). Finally, the reaction system was incubated at 37 °C in a fluorescence plate reader (Thermal Cycler Dice Real-Time System III (TaKaRa)) for 60 min, with a fluorescence measurement taken every minute. The crRNA, FQC6 probe, and target DNA sequences used in these experiments are listed in Supplementary Data 1.

### Bio-layer interferometry (BLI) analysis

The binding affinity between LbCas12a and Biotin-labeled PS DNA and PO DNA (Supplementary Table 4) was analyzed using BLI on the Octet® R8 system (Sartorius). The experimental procedure included the following steps: I, incubate the streptavidin-modified probes in 1 × LbCas12a reaction buffer for 10 min; II, load 25 nM biotin-modified PS DNA or PO DNA to allow binding to the streptavidin-modified probe; III, wash the probe with 1 × LbCas12a reaction buffer; IV, capture gradient diluted LbCas12a (652 nM, 217 nM, 72 nM, 24 nM, 8 nM) with the PS DNA or PO DNA linked probe; V, dissociate the LbCas12a by using 1 × LbCas12a reaction buffer. Finally, the binding affinity was calculated based on the association and dissociation phases observed during the interaction analysis.

### Development of DNACas based on the CRISPR–Cas system

**In vitro CRISPR–Cas12a *trans*-cleavage assay.** DNA sequences listed in Supplementary Table 5 were used to establish the DNACas concept. The assay was performed as shown below. First, the DNA sequences

were incubated with the pre-assembled LbCas12a and crRNA at room temperature for 5 min. Then, a 20 μL reaction solution was prepared with a final concentration of 15 nM LbCas12a, 15 nM crRNA, 400 nM FQC6 probe, 100 pM dsDNA target, varying concentrations of the tested DNA sequences (60 nM for Fig. 2b, Fig. 2e; 20 nM, 30 nM, 40 nM, 50 nM, or 60 nM for Fig. 2f; 20 nM, 40 nM, 60 nM, 80 nM, or 100 nM for Supplementary Fig. 1), and RNase-free water in 1 × LbCas12a reaction buffer. The reaction was initiated by irradiating with a UV lamp ($\lambda$ = 365 nm, 35 W) for 1 min. Finally, the mixture was incubated in a fluorescence plate reader for 60 min at 37 °C, with a fluorescence measurement taken every minute. The crRNA, FQC6 probe, and target DNA sequences used in these experiments are the same as shown in Supplementary Data 1.

**In vitro CRISPR–Cas12a *cis*-cleavage assay.** Briefly, the DNA sequences (PC&PS DNA1, listed in Supplementary Table 5) were incubated with the pre-assembled LbCas12a and crRNA at room temperature for 5 min. Then, in a 20 μL reaction system, 250 nM LbCas12a was mixed with 250 nM crRNA, 5 μM of the tested DNA sequences, and 50 nM target DNA in 1 × LbCas12a reaction buffer. The reaction was initiated by irradiating with a UV lamp ($\lambda$ = 365 nm, 35 W) for 1 min, followed by incubation at 37 °C for 60 min and then 95 °C for 5 min. Finally, the products were analyzed using 7.5% polyacrylamide gel electrophoresis (PAGE).

**Application of DNACas to LbuCas13a.** First, the DNA sequences (PC&PS DNA 1, listed in Supplementary Table 5) were incubated with the pre-assembled LbuCas13a (Bio-Lifesci, Guangzhou, China, catalog number: M20201-0100) and crRNA at room temperature for 5 min. Then, a mixture with a final concentration of 15 nM LbuCas13a, 15 nM crRNA, 400 nM FQU5 probe, 100 pM RNA target, and 60 nM of the tested DNA sequences in 1 × PCR Buffer (TaKaRa, catalog number: 9151 A) was prepared, and the volume was adjusted to 20 μL with RNase-free water. The reaction was initiated by irradiating with a UV lamp ($\lambda$ = 365 nm, 35 W) for 1 min. The reaction system was then incubated in a fluorescence plate reader for 60 min at 37 °C, with a fluorescence measurement taken every minute.

### Universality analysis of DNACas to CRISPR–Cas system

**Application of DNACas to SpCas9.** First, the DNA sequences (PO DNA1, PS DNA1, or PC&PS DNA1 listed in Supplementary Table 5) were incubated with the pre-assembled SpCas9 (Bio-Lifesci, Guangzhou, China, catalog number: M20101-0500) and sgRNA at room temperature for 5 min. Then, a mixture with a final concentration of 55 nM SpCas9, 55 nM sgRNA, 14 nM dsDNA target, and 10 μM of the tested DNA sequences in 1 × SpCas9 reaction buffer containing 5 mM $MgCl_2$ was prepared, and the volume was adjusted to 20 μL with RNase-free water. The reaction was initiated by irradiating with a UV lamp ($\lambda$ = 365 nm, 35 W) for 1 min. And then, the reaction system was incubated at 37 °C for 60 min and 95 °C for 5 min. The products were analyzed by 7.5% PAGE.

**Application of DNACas to BrCas12b.** First, the DNA sequences (PO DNA1, PS DNA1, or PC&PS DNA1 listed in Supplementary Table 5) were incubated with the pre-assembled BrCas12b (Bio-Lifesci, Guangzhou, China, catalog number: M20503-0500) and sgRNA at room temperature for 5 min. Then, BrCas12b *trans*-cleavage activity was measured in a 20 μL reaction system with 15 nM BrCas12b,15 nM sgRNA, 60 nM of the tested DNA sequences, 1 nM dsDNA target, and 400 nM FQT12 in 1 × BrCas12b reaction buffer. The 1 × BrCas12b reaction buffer consisted of 10 mM Tris-HCl (pH9.0), 3.5 mM $MgSO_4$, 10 mM $(NH_4)_2SO_4$, 0.1% Tween-20 (v/v). The reaction was initiated by irradiating with a UV lamp ($\lambda$ = 365 nm, 35 W) for 1 min. The reaction system was then incubated in a fluorescence plate reader for 60 min at 64°C, with a fluorescence measurement taken every minute.

### Experimental analysis of the work mechanism of DNACas

**Electrophoretic migration assay.** PAGE was performed to assess the binding affinity and stability of the FAM-labeled DNA probe (the FAM terminal-labeled or mid-labeled PO probe, PS probe, and PC&PS probe are shown in Supplementary Table 10) to the LbCas12a protein. A solution with a final concentration of 6 μM LbCas12a and 6 μM FAM-labeled-DNA probe in 1 × LbCas12a reaction buffer was prepared, and the volume was adjusted to 10 μL with RNase-free water. The mixture was incubated at room temperature or 95 °C for 5 min and then irradiated with or without a UV lamp. Finally, the products were analyzed using 10.5% PAGE.

**Fluorescence polarization assay.** A fluorescence polarization assay was performed in a 100 μL reaction with 50 nM LbCas12a, 50 nM FAM-labeled probe (listed in Supplementary Table 10) in 1 × reaction buffer (150 mM KCl, 20 mM Tris-HCl (pH7.5), 5 mM $MgCl_2$, 1 mM DTT)[59]. The mixture was incubated at room temperature for 5 min and then irradiated with or without a UV lamp. The fluorescence polarization signal of the mixture was measured using a SpectraMax iD5 Multimode Microplate Reader (Molecular Devices, CA, USA).

**Protein thermostability shift analysis.** The protein thermostability shift analysis was performed using the Protein Thermal Shift Dye Kit (Thermo Fisher Scientific, catalog number: 4461146). Briefly, a mixture with a final concentration of 400 nM LbCas12a, 800 nM tested DNA sequences (PO DNA1, PS DNA1, or PC&PS DNA1 listed in Supplementary Table 5), and 1 × Protein Thermal Shift Dye in 1 × Protein Thermal Shift buffer was prepared, and the volume was adjusted to 20 μL with RNase-free water. The mixture was then irradiated with or without a UV lamp. Finally, the solution was transferred to the QuantStudio 5 Real-Time PCR system (Thermo Fisher Scientific) for signal recording, and the reaction program was set up according to the manufacturer's protocol.

### Structural basis analysis of DNACas

**Size exclusion chromatography (SEC).** The LbCas12a protein was purified before the SEC assays. To reconstitute LbCas12a-crRNA-PC&PS DNA complex, LbCas12a protein, crRNA, and PC&PS DNA (20PS10PC, listed in Supplementary Table 11) were mixed at a molar ratio of 1:1.2:2 in 1 × LbCas12a reaction buffer and heated at 37 °C for 10 min. The mixture was applied to a Superdex 200 increase 30/100 (Cytiva) column equilibrated with buffer (50 mM Tris-HCl, pH 8.0, 150 mM KCl, 1 mM DTT). The peak fractions were polled and concentrated to ~1 mg/mL. To reconstitute LbCas12a-crRNA-PC&PS DNA complex with light irradiation, the mixture was irradiated with a UV lamp ($\lambda$ = 365 nm, 35 W) for 1 min before the SEC assay.

**Cryo-EM.** For cryo-electron microscopy (cryo-EM) sample preparation, 3 μL aliquots of the protein sample were loaded onto glow-discharged (30 s, 15 mA; Pelco easiGlow, Ted Pella) Au grids (Quantifoil, Au R1.2/1.3, 300 mesh). The grids were blotted for 5.0 s with 3 forces after waiting for 5 s and immersed in liquid ethane using Vitrobot (Mark IV, Thermo Fisher Scientific) in 100% humidity and 8 °C.

Cryo-EM data were collected at a nominal magnification of 215 K (resulting in a calibrated pixel size of 0.57 Å) on a Titan Krios (Thermo Fisher Scientific) operating at 300 kV equipped with a K3 or Falcon4i Summit detector and GIF Quantum energy filter (slit width 20 eV) in super-resolution mode. Movie stacks were automatically acquired using EPU software. The defocus range was set from −0.9 to −1.5 μm. Each movie stack, consisting of 32 frames, was exposed for 2.72 s with a total dose of ~40 $e^-/Å^2$.

**Image processing and model building.** Data processing was carried out using the cryoSPARC suite. Patch CTF estimation was carried out after alignment and summary of all 32 frames in each stack using the

patch motion correction. Initial particles were picked from a few micrographs using blob picker in cryoSPARC, and 2D averages were generated. Final particle picking was done by template picker using templates from those 2D results. After three rounds of 2D classification, ab-initio reconstruction, non-uniform refinement, and local refinement for reconstructing the density map. All maps were low-pass filtered to the map-model FSC value. The reported resolutions were based on the FSC = 0.143 criterion. An initial model was generated by Cpf1/crRNA Complex (5ID6). Then, we manually completed and refined the model using Coot. Subsequently, the models were refined against the corresponding maps by PHENIX. PyMol and UCSF Chimera were used for structural analysis and graphics generation.

### Collection and extraction of clinical samples

The nucleic acids of SARS-CoV-2 clinical samples were extracted using the QIAamp Viral RNA Mini Kit (Qiagen, catalog number: 52906) following the manufacturer's instructions, and the resulting products were stored at −80 °C for further analysis. The nucleic acids of EBV clinical samples were extracted using the QIAamp DNA Blood Mini Kit (Qiagen, catalog number: 51104) following the manufacturer's instructions, and the resulting products were stored at −80 °C for further analysis.

### Detection of clinical samples by RT-qPCR/qPCR assay

The CFDA-approved COVID-19 (SARS-CoV-2) Nucleic Acid Test Kit (Wuhan Easydiagnosis Biomedicine) was employed for the RT-qPCR assay. This involved preparing a 12.5 μL reaction mixture containing 10 μL RT-qPCR reaction solution and 2.5 μL RNA template. The mixture was then loaded into the qPCR instrument, and the thermal cycling program was set as follows: an initial reverse transcription step at 50 °C for 5 min and pre-denaturation step at 95 °C for 30 s, followed by 42 cycles of amplification reactions with denaturation at 95 °C for 3 s and annealing at 60 °C for 30 s. The fluorescence signals from each cycle were captured using the CFX96 Touch Deep Well Real-time PCR Detection System (Bio-Rad). The criteria in this nucleic acid test kit are claimed as $C_t < 38$ is positive, and $C_t \geq 38$ is negative.

The EBV DNA Quantitative Fluorescence Diagnostic Kit (Sansure Biotech) was employed for the qPCR assay. This involved preparing a 12.5 μL reaction mixture containing 9.5 μL PCR reaction solution, 0.5 μL enzyme mixture, and 2.5 μL DNA template. The mixture was then loaded into the qPCR instrument, and the thermal cycling program was set as follows: an initial denaturation step at 94 °C for 5 min, followed by 45 cycles of amplification reactions with denaturation at 94 °C for 15 s and annealing at 57 °C for 30 s. The fluorescence signals from each cycle were captured using the Thermal Cycler Dice Real Time System III (TaKaRa).

### One-pot LAMP-BrCas12b detection method

For the light-controlled one-pot LAMP-BrCas12b detection method, LAMP reaction components, CRISPR reaction components, and PC&PS DNA1 (listed in Supplementary Table 5) were included in the reaction system. The detailed procedure is shown below. First, the PC&PS DNA1 was incubated with the pre-assembled BrCas12b and sgRNA at room temperature for 5 min. Then, a one-pot LAMP-BrCas12b assay was executed in a 25 μL reaction system with a final concentration of 30 nM BrCas12b, 30 nM sgRNA, 120 nM PC&PS DNA1, 2.8 μM Bst DNA polymerase (Bio-Lifesci, Guangzhou, China, catalog number: M22101-5000), 4 U/mL Pyrophosphatase, Inorganic (yeast) (NEB, catalog number: M2403L), 400 nM FQT12, 200 nM F3/B3 primers, 1.6 μM FIP/BIP primers, 400 nM Loop F/B primers, 6 mM $MgSO_4$ (NEB, catalog number: B1003S), 1.4 mM dNTP mix (Sangon, catalog number: A610056), and 2 μL template in 1 × BrCas12b reaction buffer. The mixture was transferred into the Thermal Cycler Dice Real-Time System III for LAMP at 60 °C for 30 min. Subsequently, the mixture was irradiated for 1 min with a UV lamp ($\lambda$ = 365 nm, 35 W). Then, the mixture was incubated at 60 °C for another 60 min, and the fluorescence signal of the mixture was monitored with a fluorescence plate reader.

In the conventional one-pot LAMP-BrCas12b detection method, the components and experimental procedures resembled those detailed above, except for the absence of PC&PS DNA1 in the reaction system and the omission of UV treatment.

For the detection of SARS-CoV-2 clinical samples, a pre-reverse transcription step was required to convert RNA into cDNA. The detailed experimental process is shown below. First, a 6.5 μL reaction mixture was prepared with 0.5 μL 2 μM RT-primer-F, 0.5 μL 2 μM RT-primer-R, 0.5 μL 10 mM dNTPmix (10 mM each), and 2 μL SARS-CoV-2 clinical samples. The mixture was incubated at 65 °C for 5 min to anneal primer to template RNA. Then, a 3.5 μL RT reaction mixture containing 2 μL 5 × SSIV Buffer (Thermofisher), 0.5 μL 100 mM DTT (Thermofisher), 0.5 μL Recombinant RNase inhibitor (40 U/μL, TaKaRa, catalog number: 2313 A), and 0.5 μL SuperScript IV reverse transcriptase (200 U/μL, Thermofisher, catalog number: 18090200) was added to the annealed RNA. The mixture was incubated at 53 °C for 10 min and 80 °C for 10 min to obtain cDNA of SARS-CoV-2 clinical sample. Finally, these clinical samples were detected by the one-pot LAMP-BrCas12b detection assay; the procedure was the same as described above.

### Spatiotemporal control of gene editing in zebrafish embryos with DNACas

**Zebrafish maintenance.** Wild-type zebrafish strain AB were raised and maintained at 28.5 °C on a 14 h light/10 h dark cycle and staged according to the description[60]. The selection of mating pairs (4–10 months) was random from a pool of 15 males and 15 females.

**DNACas preparation, microinjection and image acquisition.** EasyEdit gRNAs were synthesized by GenScript with chemical modifications comprising MS at both ends. Target sequences are listed in Supplementary Table 12. To prepare the Cas9 ribonucleoprotein (RNP) complex, individual gRNA was incubated with Cas9 protein (Novoprotein, catalog number: E365-02A) at a molar ratio 1.2:1 in the reaction buffer at 37 °C for 10 min. Then RNP complex was incubated with PC&PS DNA at a molar ratio 1:2–1:4 at room temperature for 10 min. One-cell stage zebrafish embryos were injected with 2 nL of a solution containing different ratio of Cas9 RNP complex and 6 μM PC&PS DNA (26PS8PC, listed in Supplementary Table 12) to explore the optimal molar concentration. The injected embryos were then irradiated with a UV lamp ($\lambda$ = 365 nm, 35 W) for 1 min at different stages. At 2 dpf, embryos were anaesthetized with 0.03% Tricaine (Sigma-Aldrich, catalog number: E10521) and mounted in 4% methylcellulose. Images were taken by microscope (Aosvi) with MTR3CMOS camera (Sony) and edited by Adobe Photoshop CC software.

**Spatially restricted DNACas.** The embryos were injected with RNP and 26PS8PC (listed in Supplementary Table 12) as previously described and were left in the dark until developing to 6-somite (12 h post-fertilization (hpf)). Then one eye of the embryo was irradiated using a 405 nm laser in a confocal microscope (Zeiss) for 1 min. At 2 dpf, embryos were anaesthetized to acquire images and analyzed indels in the head and tail regions of the same embryos[23].

**Indels mutation analysis.** Genomic DNA was extracted from three pools, each containing six randomly collected. The targeted locus with 200–500 bp length was amplified using Fast HSTaq StarMix (GenStar, catalog number: A033-01) with the primers in Supplementary Table 12 and purified for Sanger sequencing. Then the Sanger sequencing data were analyzed by the online CRISPR analysis tool-Inference of CRISPR Edits (Synthego Co.)[61].

**RNA-seq and data analysis.** To profile transcriptional changes through RNA-seq, we collected three independent biological replicates (15 embryos per replicate) at 24 hpf following UV irradiation or microinjection treatments. Each sample was homogenized in 1 mL TRNzol reagent (TIANGEN, catalog number: DP424) following the manufacturer's protocol. RNA purity and quantity were determined with a Nanodrop-2000 spectrophotometer (Thermo Fisher Scientific), with selection criteria requiring: minimum concentration of 200 ng/μL, RNA integrity number (RIN) ≥ 7, and 28S/18S ribosomal RNA ratio ≥ 1.0. Polyadenylated mRNA was enriched using oligo(dT) magnetic beads, then fragmented into 200–700 nucleotide segments. First-strand cDNA synthesis was performed with random hexamer primers, followed by second-strand synthesis. The double-stranded cDNA underwent end-repair, 3′-adenylation, and adapter ligation. After purification with a Quick PCR extraction kit, libraries were amplified by PCR and sequenced on the Illumina HiSeqTM platform. RNA-seq data analysis was conducted using established bioinformatics pipelines.

In the RNA-seq data processing pipeline, cleaned FASTQ files were aligned to the zebrafish reference genome GRCz11 using HISAT2 (v2.2.1). Gene-level read quantification was performed with featureCounts employing the parameters -t exon and -g gene_id. Since all samples were from the same batch and the data were evaluated via box plots, density plots, and violin plots, potential batch effects were excluded from affecting the experimental results. For the exploration analysis, the gene expression matrix was first subjected to a Hellinger transformation using the decostand() function in the vegan package, and then principal component analysis (PCA) was performed on the transformed data using the rda() function to extract the principal components and their contributions, thereby enabling a visual assessment of sample distribution and clustering trends. Differential expression analysis was executed in DESeq2 with stringent thresholds ($|\log_2 FC| > 1$, adjusted $p < 0.001$), followed by MA plot visualization using plotMA() to validate expression dynamics.

### Universality analysis of DNACas for other enzymes

**Application of DNACas to T7 RNA polymerase.** First, the DNA sequences (PO DNA1, PS DNA1, or PC&PS DNA1 listed in Supplementary Table 5) were pre-incubated with T7 RNA polymerase (Bio-Lifesci, Guangzhou, China, catalog number: M20701-25000) at room temperature for 5 min. Then, in a 100 μL reaction system, 200 nM T7 RNA polymerase was mixed with 2 mM NTP mixture (Sangon, catalog number: B600057), 1 U/μL recombination RNase inhibitor, 50 nM DNA template, and 400 nM of the tested sequences in 1 × T7 RNA polymerase Buffer (40 mM Tris-HCl (pH7.5), 6 mM $MgCl_2$, 2 mM Spermidine HCl, 5 mM NaCl, 1 mM DTT). The mixture was initiated by irradiating with a UV lamp ($\lambda$ = 365 nm, 35 W) for 1 min and incubated overnight at 37°C. The products were analyzed by 2% agarose gel electrophoresis.

### Application of DNACas to RNase A

A reaction system was prepared with 0.5 μL 10 mg/mL RNase A (TaKaRa, catalog number: 2158) and 2 μL 125 μM DNA sequences (PO DNA1, PS DNA1, or PC&PS DNA1 listed in Supplementary Table 5) and incubated at room temperature for 5 min. Then, 2 μL 60 μM RNA template was added to the above reaction solution, and the volume was adjusted to 20 μL with RNase-free water. The mixture was irradiated with or without a UV lamp ($\lambda$ = 365 nm, 35 W) for 1 min. Finally, the mixture was heated at 37 °C for 10 min and then analyzed by 2% agarose gel electrophoresis.

**Application of DNACas to restriction endonuclease (Nde I).** A reaction system was prepared with 5 μL QuickCut Nde I (TaKaRa, catalog number: 1621), 2.5 μL 10 × QuickCut Buffer (TaKaRa), and 2.5 μL 40 μM DNA sequences (PO DNA1, PS DNA1, or PC&PS DNA1 listed in Supplementary Table 5) and incubated at room temperature for 5 min. Then, 5 μL 1 μM DNA targets were added to the above reaction solution, and the volume was adjusted to 25 μL with RNase-free water. The mixture was irradiated with or without a UV lamp ($\lambda$ = 365 nm, 35 W) for 1 min. Finally, the mixture was heated at 37 °C for 10 min, 75 °C for 15 min, and followed by 10.5% PAGE analysis.

### DNACas mediated light-controlled CRISPR–Cas13 assay

The detailed experimental procedures of the DNACas-mediated light-controlled CRISPR–Cas13 assay are shown below. First, the PC&PS DNA1 listed in Supplementary Table 5 was incubated with the pre-assembled LbuCas13a and crRNA at room temperature for 5 min. Then, a mixture with a final concentration of 15 nM LbuCas13a, 15 nM crRNA, 2.5 μM FQU5 probe, different concentrations of RNA target (1000 pM, 500 pM, 100 pM, 50 pM, 10 pM, 5 pM, 1 pM), and 60 nM PC&PS DNA1 in 1 × PCR Buffer was prepared at room temperature, and the volume was adjusted to 20 μL with RNase-free water. The reaction was initiated by irradiating with a UV lamp ($\lambda$ = 365 nm, 35 W) for 1 min. The reaction system was then incubated in a fluorescence plate reader for 60 min at 37 °C, with fluorescence measurements taken every minute.

In the conventional CRISPR–Cas13 assay, the components and experimental procedures resembled those detailed above, except for the absence of PC&PS DNA1 in the reaction system and the omission of UV treatment.

### DNACas mediated light-controlled CRISPR–Cas12 assay

The detailed experimental procedures of the DNACas-mediated light-controlled CRISPR–Cas12 assay are shown below. First, the PC&PS DNA1 listed in Supplementary Table 5 was incubated with the pre-assembled LbCas12a and crRNA at room temperature for 5 min. Then, a mixture with a final concentration of 15 nM LbCas12a, 15 nM crRNA, 2.5 μM FQC6 probe, different concentrations of DNA target (1000 pM, 500 pM, 100 pM, 50 pM, 10 pM, 5 pM, 1 pM), and 60 nM PC&PS DNA1 in 1 × LbCas12a reaction buffer was prepared at room temperature, and the volume was adjusted to 20 μL with RNase-free water. The reaction was initiated by irradiating with a UV lamp ($\lambda$ = 365 nm, 35 W) for 1 min. The reaction system was then incubated in a fluorescence plate reader for 60 min at 37 °C, with a fluorescence measurement taken every minute.

In the conventional CRISPR–Cas12 assay, the components and experimental procedures resembled those detailed above, except for the absence of PC&PS DNA1 in the reaction system and the omission of UV treatment.

### Statistics and reproducibility

GraphPad Prism 9 and Microsoft Excel 2021 were used for data analysis. Statistical analyses were determined using an unpaired Student's *t*-test. Significance was defined as $^{*}p < 0.05$; $^{**}p < 0.01$; $^{***}p < 0.001$; and $^{****}p < 0.0001$. All the statistical details of the experiments can be found in the figure legends. Unless otherwise stated, all experimental results were presented as mean ± standard error ($n$ = 3 technical replicates). No statistical method was used to predetermine the sample size. No data were excluded from any of the experiments. The experiments were not randomized. The investigators were not blinded to allocation during experiments and outcome assessment.

The cleavage rate was calculated according to the formula:

$$\text{Cleavage rate} = \frac{E60 - E1}{C60 - C1} \times 100\%$$

Where E60 is the fluorescence signal intensity at 60 min in the experimental group, E1 is the fluorescence signal intensity at 1 min in the experimental group, C60 is the fluorescence signal intensity at

60 min in the control group, and C1 is the fluorescence signal intensity at 1 min in the control group.

The activity recovery was calculated according to the formula:

$$\text{Activity recovery} = \frac{S_e}{S_C} \times 100\% = \frac{(EF_{T_}EF_1) \div (T-1)}{(CF_{T_}CF_1) \div (T-1)} \times 100\%$$

Where $S_e$ is the reaction rate in the experimental group, $S_c$ is the reaction rate in the control group, $EF_T$ is the fluorescence intensity at T min in the experimental group, $EF_1$ is the fluorescence intensity at 1 min in the experimental group, $CF_T$ is the fluorescence signal intensity at T min in the control group, $CF_1$ is the fluorescence signal intensity at 1 min in the control group, T is the reaction time.

The activity recovery of LbuCas13a protein was calculated using a T of 5 min. The activity recovery of other CRISPR enzymes was calculated using a T of 30 min.

The reaction velocity for the DNACas-mediated light-controlled CRISPR–Cas assay was calculated according to the formula:

$$\text{Reaction velocity} = \frac{\Delta F}{\Delta T} = \frac{EF_{T_}EF_1}{T-1}$$

Where ΔF indicates the change in the fluorescence intensity, and ΔT is the corresponding time frame. $EF_T$ is the fluorescence intensity at T min in the experimental group, and $EF_1$ is the fluorescence signal intensity at 1 min. For the high-concentration target, the fluorescence intensity before reaching the plateau was selected as the $EF_T$. In contrast, for the low-concentration target that cannot reach the plateau within 30 min, the fluorescence intensity at 30 min was used as the $EF_T$.

### Reporting summary

Further information on research design is available in the Nature Portfolio Reporting Summary linked to this article.

## Data availability

RNA-seq data are available from the National Center for Biotechnology Information Sequencing Read Archive (SRA) database, accession code PRJNA1249431. All data supporting the findings of this study are available within the article and Supplementary Information files. Source data are provided with this paper.

## References


1. Kaminski, M. M., Abudayyeh, O. O., Gootenberg, J. S., Zhang, F. & Collins, J. J. CRISPR-based diagnostics. *Nat. Biomed. Eng.* **5**, 643–656 (2021).
2. Sander, J. D. & Joung, J. K. CRISPR-Cas systems for editing, regulating and targeting genomes. *Nat. Biotechnol.* **32**, 347–355 (2014).
3. Chertow, D. S. Next-generation diagnostics with CRISPR. *Science* **360**, 381–382 (2018).
4. Wang, J. Y. & Doudna, J. A. CRISPR technology: a decade of genome editing is only the beginning. *Science* **379**, eadd8643 (2023).
5. Liu, G., Lin, Q., Jin, S. & Gao, C. The CRISPR-Cas toolbox and gene editing technologies. *Mol. Cell* **82**, 333–347 (2022).
6. Broughton, J. P. et al. CRISPR-Cas12-based detection of SARS-CoV-2. *Nat. Biotechnol.* **38**, 870–874 (2020).
7. Hu, M. et al. Photocontrolled crRNA activation enables robust CRISPR-Cas12a diagnostics. *Proc. Natl. Acad. Sci. USA***119**, e2202034119 (2022).
8. Hu, M. et al. Light-start CRISPR-Cas12a reaction with caged crRNA enables rapid and sensitive nucleic acid detection. *Angew. Chem. Int. Ed.* **62**, e202300663 (2023).
9. Chen, Y. et al. Photoactivatable CRISPR/Cas12a strategy for one-pot DETECTR molecular diagnosis. *Anal. Chem.* **94**, 9724–9731 (2022).
10. Modell, A. E., Siriwardena, S. U., Shoba, V. M., Li, X. & Choudhary, A. Chemical and optical control of CRISPR-associated nucleases. *Curr. Opin. Chem. Biol.* **60**, 113–121 (2021).
11. Zhou, W. & Deiters, A. Conditional control of CRISPR/Cas9 function. *Angew. Chem. Int. Ed.* **55**, 5394–5399 (2016).
12. Nunez, J. K., Harrington, L. B. & Doudna, J. A. Chemical and biophysical modulation of Cas9 for tunable genome engineering. *ACS Chem. Biol.* **11**, 681–688 (2016).
13. Zhuo, C. et al. Spatiotemporal control of CRISPR/Cas9 gene editing. *Signal Transduct. Target Ther.* **6**, 238 (2021).
14. Nihongaki, Y., Otabe, T. & Sato, M. Emerging approaches for spatiotemporal control of targeted genome with inducible CRISPR-Cas9. *Anal. Chem.* **90**, 429–439 (2018).
15. Gangopadhyay, S. A. et al. Precision control of CRISPR-Cas9 using small molecules and light. *Biochemistry* **58**, 234–244 (2019).
16. Nihongaki, Y., Otabe, T., Ueda, Y. & Sato, M. A split CRISPR-Cpf1 platform for inducible genome editing and gene activation. *Nat. Chem. Biol.* **15**, 882–888 (2019).
17. Hemphill, J., Borchardt, E. K., Brown, K., Asokan, A. & Deiters, A. Optical control of CRISPR/Cas9 gene editing. *J. Am. Chem. Soc.* **137**, 5642–5645 (2015).
18. Nihongaki, Y., Kawano, F., Nakajima, T. & Sato, M. Photoactivatable CRISPR-Cas9 for optogenetic genome editing. *Nat. Biotechnol.* **33**, 755–760 (2015).
19. Hoffmann, M. D. et al. Optogenetic control of Neisseria meningitidis Cas9 genome editing using an engineered, light-switchable anti-CRISPR protein. *Nucleic Acids Res.* **49**, e29 (2021).
20. Liu, Y. et al. Very fast CRISPR on demand. *Science* **368**, 1265–1269 (2020).
21. Zou, R. S., Liu, Y., Wu, B. & Ha, T. Cas9 deactivation with photocleavable guide RNAs. *Mol. Cell* **81**, 1553–1565 e1558 (2021).
22. Jain, P. K. et al. Development of light-activated CRISPR using guide RNAs with photocleavable protectors. *Angew. Chem. Int. Ed.* **55**, 12440–12444 (2016).
23. Moroz-Omori, E. V. et al. Photoswitchable gRNAs for Spatiotemporally controlled CRISPR-Cas-based genomic regulation. *ACS Cent. Sci.* **6**, 695–703 (2020).
24. Zhou, W. et al. Spatiotemporal control of CRISPR/Cas9 function in cells and zebrafish using light-activated guide RNA. *Angew. Chem. Int. Ed.* **59**, 8998–9003 (2020).
25. Zhang, Y. et al. Optical Control of a CRISPR/Cas9 System for Gene Editing by Using Photolabile crRNA. *Angew. Chem. Int. Ed.* **59**, 20895–20899 (2020).
26. Crooke, S. T., Vickers, T. A. & Liang, X. H. Phosphorothioate modified oligonucleotide-protein interactions. *Nucleic Acids Res.* **48**, 5235–5253 (2020).
27. Hyjek-Skladanowska, M. et al. Origins of the increased affinity of phosphorothioate-modified therapeutic nucleic acids for proteins. *J. Am. Chem. Soc.* **142**, 7456–7468 (2020).
28. Mou, T. C., Gray, C. W., Terwilliger, T. C. & Gray, D. M. Ff gene 5 protein has a high binding affinity for single-stranded phosphorothioate DNA. *Biochemistry* **40**, 2267–2275 (2001).
29. Li, B. et al. CRISPR-Cas12a possesses unconventional DNase activity that can be inactivated by synthetic oligonucleotides. *Mol. Ther. Nucleic Acids* **19**, 1043–1052 (2020).
30. Li, B. et al. Synthetic oligonucleotides inhibit CRISPR-Cpf1-mediated genome editing. *Cell Rep.* **25**, 3262–3272 (2018).
31. Hu, M., Wang, Y. & Zhou, X. Photochemical regulatory strategies for nucleic acid function and their biomedical applications. *Interdiscip. Med.* **2**, e20240006 (2024).

32. Ordoukhanian, P. & Taylor, J. S. Design and synthesis of a versatile photocleavable DNA building-block - application to phototriggered hybridization. *J. Am. Chem. Soc.* **117**, 9570–9571 (1995).
33. O'Hagan, M. P. et al. Photocleavable ortho-nitrobenzyl-protected DNA architectures and their applications. *Chem. Rev.* **123**, 6839–6887 (2023).
34. Carlson-Stevermer, J. et al. CRISPRoff enables spatio-temporal control of CRISPR editing. *Nat. Commun.* **11**, 5041 (2020).
35. Wang, L. et al. Phosphorothioation of DNA in bacteria by dnd genes. *Nat. Chem. Biol.* **3**, 709–710 (2007).
36. Eckstein, F. Phosphorothioates, essential components of therapeutic oligonucleotides. *Nucleic Acid Ther.* **24**, 374–387 (2014).
37. Crooke, S. T., Liang, X. H., Baker, B. F. & Crooke, R. M. Antisense technology: a review. *J. Biol. Chem.* **296**, 100416 (2021).
38. Crooke, S. T., Wang, S., Vickers, T. A., Shen, W. & Liang, X. H. Cellular uptake and trafficking of antisense oligonucleotides. *Nat. Biotechnol.* **35**, 230–237 (2017).
39. Seth, P. P., Tanowitz, M. & Bennett, C. F. Selective tissue targeting of synthetic nucleic acid drugs. *J. Clin. Investig.* **129**, 915–925 (2019).
40. Gaus, H. J. et al. Characterization of the interactions of chemically-modified therapeutic nucleic acids with plasma proteins using a fluorescence polarization assay. *Nucleic Acids Res.* **47**, 1110–1122 (2019).
41. Zhang, L., Vickers, T. A., Sun, H., Liang, X. H. & Crooke, S. T. Binding of phosphorothioate oligonucleotides with RNase H1 can cause conformational changes in the protein and alter the interactions of RNase H1 with other proteins. *Nucleic Acids Res.* **49**, 2721–2739 (2021).
42. Liang, X. H. et al. Hsp90 protein interacts with phosphorothioate oligonucleotides containing hydrophobic 2′-modifications and enhances antisense activity. *Nucleic Acids Res.* **44**, 3892–3907 (2016).
43. Hyjek-Skladanowska, M. et al. Structures of annexin A2-PS DNA complexes show dominance of hydrophobic interactions in phosphorothioate binding. *Nucleic Acids Res.* **51**, 1409–1423 (2023).
44. Chen, J. S. et al. CRISPR-Cas12a target binding unleashes indiscriminate single-stranded DNase activity. *Science* **360**, 436–439 (2018).
45. Gootenberg, J. S. et al. Nucleic acid detection with CRISPR-Cas13a/C2c2. *Science* **356**, 438–442 (2017).
46. Tian, Y. et al. A novel thermal Cas12b from a hot spring bacterium with high target mismatch tolerance and robust DNA cleavage efficiency. *Int. J. Biol. Macromol.* **147**, 376–384 (2020).
47. Ericsson, U. B., Hallberg, B. M., Detitta, G. T., Dekker, N. & Nordlund, P. Thermofluor-based high-throughput stability optimization of proteins for structural studies. *Anal. Biochem.* **357**, 289–298 (2006).
48. Tong, X. et al. Fast and sensitive CRISPR detection by minimized interference of target amplification. *Nat. Chem. Biol.* **20**, 885–893 (2024).
49. Lu, S. et al. Fast and sensitive detection of SARS-CoV-2 RNA using suboptimal protospacer adjacent motifs for Cas12a. *Nat. Biomed. Eng.* **6**, 286–297 (2022).
50. Busson, P., Keryer, C., Ooka, T. & Corbex, M. EBV-associated nasopharyngeal carcinomas: from epidemiology to virus-targeting strategies. *Trends Microbiol.* **12**, 356–360 (2004).
51. Chan, K. C. A. et al. Analysis of plasma Epstein-Barr virus DNA to screen for nasopharyngeal cancer. *N. Engl. J. Med.* **377**, 513–522 (2017).
52. Cohen, J. I. Epstein-Barr virus infection. *N. Engl. J. Med.* **343**, 481–492 (2000).
53. Young, L. S. & Rickinson, A. B. Epstein-Barr virus: 40 years on. *Nat. Rev. Cancer* **4**, 757–768 (2004).
54. Jao, L. E., Wente, S. R. & Chen, W. Efficient multiplex biallelic zebrafish genome editing using a CRISPR nuclease system. *Proc. Natl. Acad. Sci. USA***110**, 13904–13909 (2013).
55. Liang, X. H., Shen, W., Sun, H., Prakash, T. P. & Crooke, S. T. TCP1 complex proteins interact with phosphorothioate oligonucleotides and can co-localize in oligonucleotide-induced nuclear bodies in mammalian cells. *Nucleic Acids Res.* **42**, 7819–7832 (2014).
56. Mou, T. C. & Gray, D. M. The high binding affinity of phosphorothioate-modified oligomers for Ff gene 5 protein is moderated by the addition of C-5 propyne or 2′-O-methyl modifications. *Nucleic Acids Res.* **30**, 749–758 (2002).
57. Gao, W. Y., Han, F. S., Storm, C., Egan, W. & Cheng, Y. C. Phosphorothioate oligonucleotides are inhibitors of human DNA polymerases and RNase H: implications for antisense technology. *Mol. Pharmacol.* **41**, 223 (1992).
58. Liang, X. H., Sun, H., Shen, W. & Crooke, S. T. Identification and characterization of intracellular proteins that bind oligonucleotides with phosphorothioate linkages. *Nucleic Acids Res.* **43**, 2927–2945 (2015).
59. Maji, B. et al. A high-throughput platform to identify small-molecule inhibitors of CRISPR-Cas9. *Cell* **177**, 1067–1079 (2019).
60. Kimmel, C. B., Ballard, W. W., Kimmel, S. R., Ullmann, B. & Schilling, T. F. Stages of embryonic development of the zebrafish. *Dev. Dyn.* **203**, 253–310 (1995).
61. Conant, D. et al. Inference of CRISPR edits from Sanger trace data. *CRISPR J.* **5**, 123–130 (2022).


## Acknowledgements

This work was supported by National Key R&D Program of China (2023YFC2307400 to X.M.Z.), grants from the National Natural Science Foundation of China (32150019 to X.M.Z., 32300692 to F.L., 92068201 to D.Q.P.), the Basic and Applied Basic Research Foundation of Guangdong Province (2021A1515220164 to X.M.Z., 2025A1515011002 to M.L.H., 2025A1515012118 to F.L.), China Postdoctoral Science Foundation (2024M760985 to M.L.H., GZB20240235 to M.L.H., 2024T170292 to F.L., 2023M741235 to F.L.), and the Key R&D Program of Zhejiang (2024SSYS0035 to Westlake Laboratory). This study was supported in part by the InnoHK initiative of the Innovation and Technology Commission of the Hong Kong Special Administrative Region Government (to Y.Y.S.).

## Author contributions

M.L.H., B.N.Z., and X.M.Z. conceived the study. X.M.Z., M.L.H., D.Q.P., and F.L. supervised the study. M.L.H., B.N.Z., Y.Y.S., F.C., Y.H.W., W.W.Q., X.W., X.Y.G., and M.M.Z. performed the experiments and contributed to the data analysis and management. Y.T.S., W.X., and T.T. assisted in conducting the CRISPR experiments. M.L.H., B.N.Z., Y.Y.S., F.L., M.F.Z., D.Q.P., and X.M.Z. were involved in the data interpretation, discussed the results, and commented on the study. X.M.Z., M.L.H., Y.Y.S., and F.L. wrote the manuscript. All authors reviewed and approved the manuscript. These authors contributed equally: Menglu Hu, Bingni Zhang, Yuanyue Shan.

## Competing interests

M.L.H., B.N.Z., and X.M.Z. are listed as inventors on patent applications related to this work (nos. 202310085673.0, 202310085460.8, and 202310085454.2) that were submitted by South China Normal University. The remaining authors declare no competing interests.

## Additional information

**Supplementary information** The online version contains supplementary material available at https://doi.org/10.1038/s41467-025-61094-5.

**Correspondence** and requests for materials should be addressed to Mingfeng Zhang, Fang Liang, Duanqing Pei or Xiaoming Zhou.

**Peer review information** *Nature Communications* thanks the anonymous reviewers for their contribution to the peer review of this work. A peer review file is available.

**Reprints and permissions information** is available at http://www.nature.com/reprints

**Publisher's note** Springer Nature remains neutral with regard to jurisdictional claims in published maps and institutional affiliations.

**Open Access** This article is licensed under a Creative Commons Attribution-NonCommercial-NoDerivatives 4.0 International License, which permits any non-commercial use, sharing, distribution and reproduction in any medium or format, as long as you give appropriate credit to the original author(s) and the source, provide a link to the Creative Commons licence, and indicate if you modified the licensed material. You do not have permission under this licence to share adapted material derived from this article or parts of it. The images or other third party material in this article are included in the article's Creative Commons licence, unless indicated otherwise in a credit line to the material. If material is not included in the article's Creative Commons licence and your intended use is not permitted by statutory regulation or exceeds the permitted use, you will need to obtain permission directly from the copyright holder. To view a copy of this licence, visit http://creativecommons.org/licenses/by-nc-nd/4.0/.

© The Author(s) 2025